energies

MDPI

Review

Experimental Investigations of Forced Convection of Nanofluids in Smooth, Horizontal, Round Tubes: A Review

Janusz T. Cieśliński * and Przemysław Kozak

Faculty of Mechanical and Ocean Engineering, Gdańsk University of Technology, Narutowicza 11/12, 80233 Gdansk, Poland; ozariasz@go2.pl

* Correspondence: jcieslin@pg.edu.pl

Abstract: A comprehensive review of published works dealing with experimental studies of forced convection heat transfer of nanofluids is presented. The survey is limited to straight, smooth, and round tubes. Moreover, only mono nanofluids exhibiting Newtonian behaviour are considered. Works on experimental research of forced convection in tubes are presented in a chronological order in the first part of the article. In this part, attention was paid to the influence of nanoparticles on the intensification of heat transfer. Information on the tested nanofluids, the measurement technique used, and the measurement range are presented in tabular form. Correlation equations proposed by individual researchers are also presented. In order to explain the controversy regarding the different influences of nanoparticles on the intensity of heat transfer during forced convection of nanofluids, the second part of the paper presents a comparison of the test results obtained by different researchers for the same nanofluid, possibly under the same thermal and flow conditions. Finally, the main conclusions are discussed.

Keywords: mono nanofluids; forced convection; heat transfer; experiment; round; straight tubes; correlations

Citation: Cieśliński, J.T.; Kozak, P. Experimental Investigations of Forced Convection of Nanofluids in Smooth, Horizontal, Round Tubes: A Review. *Energies* **2023**, *16*, 4415. https://doi.org/10.3390/en16114415

Academic Editor: Gianpiero Colangelo

Received: 20 March 2023
Revised: 22 May 2023
Accepted: 25 May 2023
Published: 30 May 2023

1. Introduction

Since the publication of Choi's work [1] in 1995, nanofluids have been at the center of interest of many research groups around the world. In the initial period, the properties of nanofluids were studied, because nanofluids show completely different properties compared to the base fluids after adding even a small amount of nanoparticles (NPs) [2,3]. In particular, the thermal conductivity of the nanofluids, which showed a significant increase compared to the base fluid was studied intensively. The state of knowledge in this field is well presented in [4–6].

At the same time, research was conducted on the use of nanofluids, especially in systems with high heat flux such as nuclear reactors [7,8], microelectronics [9,10], gas turbines [11], car radiators [12,13], and lasers [14]. Another field of application of nanofluids is the cooling systems of vehicle engines [15], fuel cells [16,17], or thermoelectric generators [18]. High expectations are associated with the use of nanofluids in numerous solar technologies [19–21]. Particularly interesting seems to be the use of nanofluids in various types of heat exchangers [22–25]. Information on other applications of nanofluids can be found in [26–28].

In the design of all thermo-hydraulic systems, correlation equations are used to calculate heat transfer coefficients (HTC). The development of reliable equations for determining the HTC requires—apart from theoretical work—a large number of experiments. In experimental studies, the essential parameters affecting heat transfer must be taken into account. In the case of nanofluids, apart from the parameters that are essential for base fluids, such as flow velocity, temperature, heat flux, and mass flow rate, the influence of NPs concentration and their type, material, and size are also important. Due to the fact that experimental research is tedious, time-consuming, and expensive, it is reasonable to ask

whether the equations used for base fluids can also be applied to nanofluids. Therefore, it is important to critically evaluate the results obtained in different research centers.

In contrast to the reviews published so far, e.g., [29–36], this paper focuses on the results of experimental studies of heat transfer under forced convection for one geometry, i.e., for horizontal, straight, smooth, and round tubes, and nanofluids referred to as mono nanofluids or unitary nanofluids. It is also important to emphasize that the discussed nanofluids exhibit properties of Newtonian fluids.

Due to the fact that round, smooth tubes are the basic geometry used in the construction of the extremely popular shell and tube heat exchangers, the process of heat transfer during the flow inside the tubes has been studied for almost a hundred years [37–39]. Hence, the knowledge on this subject is well-established, and the proposed correlation equations are the basis for the design of heat exchangers, as well as a benchmark in modern laboratory research. Therefore, it is not surprising that there is a large number of research papers on heat transfer under conditions of forced convection of nanofluids in horizontal, smooth, and round tubes.

The aim of this paper is to create a possibly complete database obtained by researchers for various tested nanofluids and for a wide spectrum of parameters related to forced convection of nanofluids in horizontal, smooth, and round tubes. The main idea of this study is the comparison of the measurement results obtained in different research centers for the same nanofluids under the same flow conditions. The term "same nanofluid" means a nanofluid consisting of the same base fluid and nanoparticles of the same type and concentration. Unfortunately, there are too few published data to take into account such parameters as the size and shape of nanoparticles, which undoubtedly affect convective heat transfer. When comparing the results, attention was paid to the geometry of the tube, i.e., its inside diameter and active length, as well as the material from which it was made. The method of the tube heating is clearly indicated, too—see Table 1. It is important to note which thermal boundary condition corresponds to the adopted method of heat supply. In the case of electric heating, it is important whether it was direct current (DC) or alternating current (AC), because the electric field can affect surface-charged NPs. Many researchers limit themselves to the validation of the used apparatus and measurement procedure by comparing them to classical correlations for base fluids and on this basis draw conclusions about the intensification or deterioration of heat transfer in relation to the tested nanofluids. However, a reliable evaluation of the obtained results is achieved by comparing them with data from another center for a given nanofluid under specific thermal and flow conditions. To the best of the authors' knowledge, no such exhaustive comparison of measurement data on convective heat transfer of nanofluids has been published in the literature.

2. Characteristics of the Conducted Research

Pak and Cho [40] were the first to study the heat transfer of nanofluids under conditions of forced convection. It was established that the Nusselt (Nu) number increased with NP concentration and Reynolds (Re) number increase. However, for the highest examined NP concentration, HTC of the nanofluid was about 12% smaller than that of base fluid when compared for the same mean velocity. A correlation equation for turbulent regime was developed. Li and Xuan [41] found that HTC of nanofluid increased by about 60% compared to the base fluid at the same Re number. Correlation equations for laminar and turbulent regimes were developed—see Tables 2 and 3. Xuan and Li [42] established that the Nu number of the nanofluid for turbulent flow increased more than 39% compared to the base fluid. Wen and Ding [43] established that the use of NPs significantly improved heat transfer in the laminar flow regime, particularly in the entrance region. Wen and Ding [43] concluded that the presence of NPs leads to a decrease in the thermal boundary layer thickness. Yang et al. [44] observed that NPs increased the HTC in laminar flow of low Re number, but the increase is much less than that predicted by correlation equation for base fluids based on the thermal conductivity of nanofluid. Kabelac and Kuhnke [45] did not observe any systematic relationship between NPs concentration and HTC. However,

for the highest NPs concentration tested, HTC for nanofluid was lower by about 10% compared to the base fluid at the same boundary conditions. Heris et al. [46] observed heat transfer enhancement with an increase in NPs concentration and Peclet (Pe) number, after which, for the optimal value of NPs concentration, HTC decreased. Heris et al. [47] determined that HTC increased with increasing concentration of NPs and Pe number with a maximum of about 43%. Ding et al. [48] observed enormous local HTC improvement, of about 350%, during laminar flow and relatively small NPs concentration, which could not be attributed purely to the thermal conductivity enhancement. Moreover, the effect of pH on heat transfer of nanofluids was investigated for the first time. Heris et al. [49] found that HTC of nanofluid increased with NPs concentration and Pe number increase and contrary to the observation of Yang et al. [44], was significantly higher than that calculated from a conventional correlation equation. Williams et al. [50] did not observe spectacular heat transfer enhancement during fully developed turbulent flow of nanofluid. Moreover, it was shown that correlation equations for base fluids predict HTC well, provided that thermophysical properties of nanofluids are used for calculations. Kulkarni et al. [51] established that at a fixed Re number, HTC of nanofluid increased with NP diameter increase. Sommers and Yerkes [52], like Heris et al. [47], observed the optimum concentration of NPs, for which HTC reached the maximum enhancement—about 15–20%, compared to the base fluid. Kim et al. [53] found that the HTC coefficient of nanofluids increased significantly more than their thermal conductivity and depended on the type of NPs and the flow regime. For example, for water–carbonic nanofluid, the thermal conductivity was the same as for water, and the HTC for laminar flow was 8% higher than for water. Anoop et al. [54] determined that the HTC in the laminar developing region was larger the smaller was the diameter of the NPs. In addition, like Wen and Ding [43], they observed that NPs significantly intensify the HTC in the entrance region. A correlation equation for local Nu number in the entrance region was developed—see Table 2. Yu et al. [55] showed that for turbulent flow, HTC increased by about 50–60% compared to the base fluid for the same Re number. In addition, the experimental HTC were approximately 14–32% higher than those calculated from the base fluid correlation. Liao and Liu [56] did not observe a significant effect of NPs on heat transfer for low concentrations and lower nanofluid temperature, and the Nu number calculated from the base liquid correlations did not differ from the experimental values for laminar flow. However, for turbulent flow and higher temperature of the nanofluid, the Nu number calculated from the correlation for the base fluid was lower by about 15% for laminar flow and by about 24% for turbulent flow. Hwang et al. [57] determined that for a fully developed laminar flow, HTC increased with the increase in NPs concentration by about 8%, and the use of correlation for the base fluid did not allow them to calculate this surplus. In addition, it was shown that the increase in HTC significantly exceeded the increase in thermal conductivity of nanofluids. Asirvatham et al. [58] observed that even for a very low concentration of NPs, the HTC increased by about 8% compared to the base fluid. Important parameters affecting heat transfer were the velocity and inlet temperature of the nanofluid. A correlation equation for local Nu number in the entrance region was developed—see Table 2. Torii and Yang [59] determined that HTC increased with increasing Re number and concentration of NPs. The maximum HTC rise was almost 25% in the entrance region and decreased with distance from the inlet. Sharma et al. [60] observed an increase in HTC with an increase in Re number and NPs concentration with a maximum of about 23.7%. A correlation equation was proposed for transition flow of nanofluids—see Table 3. Duangthongsuk and Wongwises [61], like Herris et al. [46] and Sommers and Yerkes [52], showed that HTC increased only for a certain value of NPs concentration, beyond which HTC decreased. The maximum increase in HTC for turbulent flow and optimum NPs concentration was about 26%, while the decrease in HTC for higher concentration of NPs was equal to 14%. Mosavian et al. [62] confirmed that, regardless of the type of NPs, there was an optimum concentration of NPs for which the maximum intensification of heat transfer was obtained during laminar flow. Fotukian and Esfahany [63] determined that the enhancement ratio of HTC during turbulent flow of nanofluid decreased with

Re number increase. Maximum increase in HTC for optimum NPs concentration was 48%. Fotukian and Esfahany [64] using the same procedures as in [63] but other types of NPs, established that HTC enhancement was about 25%. Vajjha et al. [65] conducted a comprehensive investigation for three types of NPs in a wide concentration range, which confirmed that the HTC for nanofluids was higher than for the base fluid, and also allowed the development of a more universal correlation for calculating the HTC for fully developed turbulent flow—see Table 3. Amrollahi et al. [66] studied the effect of NPs concentration and nanofluid temperature on heat transfer in the entrance region for laminar and turbulent flow. It was found that both the increase in the concentration of NPs and the temperature of the nanofluid caused the increase in HTC. Xie et al. [67] found that for laminar flow it was possible to increase the HTC by up to 252% if the appropriate type, size, and concentration of NPs was selected. Baby and Ramaprabhu [68] established that HTC enhancement in the entrance region for turbulent flow increased with Re number and NPs concentration increase and may be as high as 141% for higher tested NPs concentration. Asirvatham et al. [69] studied the influence of inlet temperature, NPs concentration, and velocity on HTC for laminar, transition, and turbulent flow of nanofluids. It was found that HTC increased with NPs concentration increase, and the maximum increase compared to the base fluid was 69.3%. The research results were generalized in the form of a correlation equation—see Table 4. Sajadi and Kazemi [70] determined that the addition of NPs resulted in a 22% increase in HTC for fully developed turbulent flow. It was significant that a five-fold increase in NPs concentration resulted in only a 3% increase in HTC. A correlation equation was proposed for transition and turbulent flow of nanofluids—see Table 3. Ferrouillat et al. [71] were the only ones who conducted research on both heating and cooling of nanofluids for several inlet temperatures in a wide range of NPs concentration. It was found that the HTC for the nanofluid was higher from 10% to 60% compared to the base fluid. It was emphasized that the correlation equations for the base fluids in which the thermophysical properties of the tested nanofluids were used correctly reproduced the experimental results. Bearing in mind that the tests for the cooling and heating cases were not carried out in identical thermal conditions, in the case of cooling the intensity of heat transfer can be defined as equal to or better than that for heating. Ho et al. [72] noted that in the entrance region HTC increased substantially compared to the base fluid, and then decreased with distance from the inlet. In addition, HTC was very sensitive to mass flow rate with a maximum increase of about 6% and practically was independent of heat flux. Timofeeva et al. [73] showed that for the same velocity of base fluid and nanofluid, HTC increased with the increase in NPs diameter, NPs concentration, and inlet temperature. For the maximum values of the mentioned parameters, the increase in HTC was 14.2%. Chandrasekar and Suresh [74] observed HTC and Nu number increase with NPs concentration and Re number increases with a maximum of about 53% and 100%, respectively. Empirical correlation equations for laminar and turbulent flow were proposed—see Tables 2 and 3. Abdulhassan et al. [75] demonstrated that the heat transfer enhancement ratio depended on the material of NPs. Nanofluids that contain metallic NPs displayed better enhancement compared to oxide nanofluids. The conducted tests showed that for metallic NPs, the increase in Nu number was 45%, while for ceramic NPs it did not exceed 32% compared to the base fluid. Shokouhi et al. [76] tested the impact of NPs concentration and Re number on heat transfer in the entrance region under laminar flow. It was established that for higher NPs concentration and the highest tested Re number, the maximum increase in HTC was 23%. Moreover, it was determined that the correlation equation for base fluid underpredicted the Nu number. Vishwanadula and Nsofor [77] found that the Nu number for nanofluid under turbulent flow was 20% higher compared to base fluid for the same Re number. A correlation for calculating the Nu number was proposed—see Table 3. Heyhat et al. [78] established that HTC increased with NPs concentration increase with a maximum of about 23%. Moreover, like Williams et al. [50], Heyhat et al. [78] found that the correlations for base fluids perfectly reflected the results for nanofluids, provided that the thermophysical properties of nanofluids were applied. Kayhani et al. [79] observed only a

slight increase in the Nu number—of about 8%—during the turbulent flow of nanofluids. Nine et al. [80] found that the HTC increased with NPs concentration increase, up to the value of about 37%, while thermal conductivity increased by about 5% for the same NPs concentration. Yu et al. [81] found that the addition of NPs caused a significant increase in HTC—up to about 108%—during laminar flow and cooling mode. Julia et al. [82] reported 300% HTC enhancement during turbulent flow of nanofluids. Despite such a significant increase in HTC, the researchers believed that the correlation equations for the base fluids can be used for the predictions of HTC for nanofluids, provided that the thermophysical properties of the nanofluid were used. Saeedinia et al. [83] found that the increase in the thermal conductivity of nanofluid with a high Prandtl (Pr) number was about 6%, while the HTC increased by about 13%. Arani and Amani [84] observed an increase in Nu number with increasing Re number and NPs concentrations with a maximum of about 80%. A correlation equation for calculating the Nu number was proposed—Table 3. Almohammadi et al. [85] found an increase in HTC with increasing Re number and NPs concentrations with a maximum of about 27%. The maximum heat transfer enhancement was recorded in the entrance region. Kumaresan et al. [86] examined the influence of the NPs concentration, the inlet temperature of the nanofluid, and the heating fluid on heat transfer both in laminar and turbulent flow in the entrance region. It was found that for the optimum combination of the three mentioned factors, HTC increased by about 150% compared to the base fluid. In addition, it was stated that the correlation equations for base fluids could not be used to calculate the HTC for nanofluids for both laminar and turbulent flow. Azmi et al. [87] like Herris et al. [46], Sommers and Yerkes [52], and Duangthongsuk and Wongwises [61] previously, observed that HTC increased only for a certain value of NPs concentration, beyond which HTC decreased. The maximum increase in Nu number for turbulent flow and optimum NPs concentration varied between 30% and 39%. Valuable information from the study of Azmi et al. [87] was that the HTC decreased when the viscosity to thermal conductivity enhancement ratio was greater than 5.0. Finally, a correlation for calculating the Nu number was proposed—see Table 3. Meyer et al. [88] showed that for turbulent flow and higher concentration of NPs, the increase in the Nu number could be as much as 33.2% compared to the base fluid for the same Re number. However, when comparing the HTC for the same velocity, the HTC for nanofluid was lower by about 12.3% compared to the base fluid. For laminar flow, a slight HTC enhancement of about 2.3% was observed. According to Meyer et al. [88], the use of nanofluids was beneficial if the ratio of viscosity increase to thermal conductivity increase did not exceed 4. Ferrouillat et al. [89] conducted experiments for two types of NPs of different shapes. A slight (8%) increase in the Nu number was observed for nanofluids with NPs with a shape factor greater than 3. Abreu et al. [90] observed an increase in the Nu number with NPs concentration increase under laminar flow with a maximum of about 47%, while the thermal conductivity enhancement was only 7.4%. Haghighi et al. [91], taking into account the criterion of the same pumping power, found that the five tested nanofluids showed a lower HTC than the base fluid under laminar flow in a small diameter tube. Moreover, the measurement results were within ±15% band while using a correlation equation for the base fluid. Paul et al. [92] found that for nanofluids with ionic base fluid, HTC increased with Re number increase with a maximum of about 15% in the entrance region under laminar flow. Sahin et al. [93] found that in turbulent flow, the addition of NPs caused an increase in HTC and Nu number compared to the base fluid. They also found that there was an optimum concentration of NPs below and above which heat transfer intensification decreased. The maximum increase in HTC was about 40%. A correlation generalizing the research results was also proposed—see Table 3. Wusiman et al. [94] studied heat transfer of nanofluids during laminar, transition, and turbulent flow. They observed that only for laminar flow was there a significant intensification of HTC, with HTC being twice as high as for the base fluid. Significant deterioration of the HTC compared to the base fluid was observed for the transition flow. For turbulent flow, HTC increased gently with increasing NPs concentration and Re number. Heyhat et al. [95] found that for a fully developed

laminar flow, the HTC increased with the increase in the Re number and NPs concentration, and the maximum rise was 32%. Feng and Li [96] revealed that adding NPs to fluids with a high Pr number significantly deteriorated heat transfer for laminar mixed convection. The decrease in HTC was higher the higher was the concentration of NPs. However, for the same Grashof (Gr) number, an increase in NPs concentration resulted in an increase in HTC. Rayatzadeh et al. [97] observed a nonmonotonic dependence of Nu number against NPs concentration. The maximum increase in Nu number was 8%, and for the highest tested concentration of NPs, a decrease in Nu number of about 1% was recorded compared to the base fluid. The use of sonication improved heat transfer intensity for each tested NPs concentration, but still in the case of the highest tested concentration of NPs, the Nu number was lower than for the other concentrations. Esmaeilzadeh et al. [98] recorded HTC increase with NPs concentration increase with a maximum of about 19% in the entrance region. A correlation equation generalizing the research results was also proposed—see Table 3. Meriläinen et al. [99] observed that the average HTC of water-based nanofluids increased by about 40% regardless of the type of NPs. Azmi et al. [100] observed that HTC enhancement depended on the type of NPs and their concentration. For the two tested types of NPs, the maximum increase in HTC was about 33%, but there was also a decrease in HTC compared to base fluid for some NPs concentration. Gupta et al. [101] recorded a significant increase in HTC—up to 50%—with an increase in NPs concentration using the same velocity criterion. However, for the highest tested NPs concentration, HTC deterioration was detected compared to the base fluid. A correlation equation was proposed for laminar flow—see Table 2. Mojarrad et al. [102] showed that the addition of NPs to the base fluid resulted in a significant increase in both HTC (up to 24%) and Nu number. However, the ratio of the Nu numbers for nanofluid and base fluid did not change as the Re number increased. A correlation equation was proposed for laminar flow—see Table 2. Chiney et al. [103] established that the addition of NPs may result in overall HTC improvement up to 54% under laminar flow in a double tube system. It was also found that the degree of intensification of the overall HTC decreased with the increase in the thermal conductivity of the heat transfer wall material. Haghighi et al. [104] evaluated the results for nanofluids using two criteria: the same Re number and the same pumping power. Using the criterion of the same Re number, the results indicated an increase in HTC by about 51% compared to the base fluid. However, comparing the results for nanofluids and base fluid using the criterion of the same pumping power showed a decrease in HTC by as much as 63%. Researchers recommended using the condition of the same pumping power as a criterion for heat transfer enhancement in nanofluid systems. Sadeghinezhad et al. [105] reported an increase in the HTC of nanofluids with a low concentration of NPs with increasing velocity and heat flux for turbulent flow. The maximum increase in HTC was about 160%. Ghozatloo et al. [106] determined that the HTC of nanofluid increased with increasing temperature and NPs concentration, while the influence of NPs on the intensification of heat transfer was more pronounced the higher was the temperature. The increase in HTC compared to base fluid for the highest tested temperature was about 36%. Halelfadl et al. [107] studied the influence of the type of base fluid, the aspect ratio of MWCNT, and the type of surfactant on heat transfer under laminar flow. It was revealed that HTC increased with the aspect ratio increase and thermal conductivity of base fluid decrease. The maximum increase in HTC was about 12% compared to base fluid. Reddy and Rao [108] determined that Nu number increased with Re number and NPs concentration increase. The maximum increase in Nu number was about 11% compared to base fluid, however the measurement error was about $\pm$10%. Ho and Lin [109] achieved the maximum increase in HTC for the minimum studied concentration of NPs, amounting to about 40%. In addition, the HTC depended heavily on the inlet temperature. With doubling the inlet temperature, the HTC increased by about 44%. Heat transfer degradation compared to base fluid was observed for the maximum tested NPs concentration. Utomo et al. [110] conducted comparative studies of heat transfer under laminar flow for the same flow rate, same velocity, same pumping power, and same Re number. The obtained results show that in all tested cases, comparing HTC

with the same Re number indicated heat transfer enhancement. In turn, the comparison of HTC with the same pumping power indicated a slight heat transfer deterioration or heat transfer enhancement depending on the aggregation of NPs. HTC comparison for the same flow rate or velocity indicated a slight heat transfer enhancement in all tested cases. Esfe et al. [111] noticed HTC increase up to 36% for the highest tested NPs concentration and intermediate Re number. Nu number increased as well—up to 22%—but, as in the study by Kayhani et al. [79], the increase did not depend on changes in the concentration of NPs. Akhavan-Zanjani et al. [112] found that the addition of even a small amount of NPs caused an increase in HTC to about 6%, which was almost constant over the entire range of the Re number. The researchers determined that the Nu number reached the optimum for the moderate Re number, for which it was slightly higher than for the base fluid, and for larger and smaller Re numbers it was lower than for the base fluid by about 8%. Sahin et al. [113] observed the optimum NPs concentration above which Nu number decreased for turbulent flow. In addition, they determined the optimum Re number for which the increase in the Nu number was the highest—about 20%. Moreover, regardless of the concentration of NPs, no improvement in heat transfer was observed for the minimum Re number tested. Akhavan-Behabadi et al. [114] found that the Nu number increased up to 26% with NPs concentration increase. Moreover, for the measured thermophysical properties of the tested nanofluids, the correlation equation for the base fluid correctly predicted the Nu number. Mehrali et al. [115] found an increase in thermal conductivity of the tested nanofluids in the range of 12% to 28%, while maximum HTC increase was only 15%. Contrary to Feng and Li [96], Amiri et al. [116] showed that the addition of even a small amount of NPs to fluid of high Pr number resulted in HTC increase of about 48% compared to base fluid at the same Re number. Colla et al. [117] showed that in the case of nanofluids whose thermal conductivity and viscosity are almost identical to those of the base fluid, the Nu number is lower by about 22%. Minakov et al. [118] showed that for the same mass flow rate, HTC of the nanofluid was about 13% higher than for the base fluid, while for the same Re number, HTC increase was about 40%. Sadeghinezhad et al. [119] found that the Nu number increased with Re number and heat flux increase even for relatively small concentrations of NPs. The maximum increase in the Nu number was about 83% compared to the base fluid at the highest tested concentration of NPs and heat flux. Chavan and Pise [120] found that HTC increased with increasing NPs concentration, and the maximum increase was 36% compared to the base fluid for the minimum Re number tested. A correlation equation generalizing the research results was also proposed—see Table 3. Usri et al. [121] observed for turbulent flow HTC increase with the increase in NPs concentration and Re number. The maximum increase in HTC was about 16% compared to the base fluid at the highest tested concentration of NPs and Re number. Cabaleiro et al. [122] did not observe any impact of NPs on heat transfer during laminar and transition flow, although thermal conductivity was enhanced by about 4%. Moreover, experimental data were reasonably reproduced by correlation equations for base fluid. Gómez et al. [123] found HTC improvement of about 6% for the same mass velocity and about 30% for the same Re number, compared to the base fluid. Patel and Subhedar [124] observed increase in the Nu number and HTC with the increase in mass flow rate and NPs concentrations for laminar flow. The maximum increase in the Nu number was 16% compared to the base fluid at the highest tested concentration of NPs and mass flow rate. Esfe et al. [125] found that for fully developed turbulent flow the maximum increase in the Nu number compared to the base fluid was about 12%. Akhavan-Zanjani et al. [126] observed that the increase in thermal conductivity and HTC compared to the base fluid was of the same order, i.e., 10% and 14%, respectively. The studied nanofluids should be treated as very diluted. Hatwar and Kriplani [127] used nonmetallic NPs with two different thermal conductivities and found that for the same concentration, the increase in HTC compared to the base fluid was higher for NPs with a higher thermal conductivity. However, while the ratio of thermal conductivity was about 1.35, the ratio of HTC increments was about 1.80. Hekmatipour et al. [128] showed that for laminar mixed flow in the developing region, the maximum increment of

the Nu number was about 18%. In addition, a correlation equation for mixed convection was proposed—see Table 2. Selvam et al. [129] studied heat transfer of nanofluids during laminar, transition, and turbulent flow. Contrary to Wusiman et al. [94], Selvam et al. [129] determined significant heat transfer intensification in the transition and turbulent regime with maximum HTC enhancement of about 42%. Zarringhalam et al. [130] determined that HTC and Nu number increased with NPs concentration an Re number increase. The highest increases in both HTC and Nu number were observed for the minimum tested Re number, and were 57% and 27%, respectively. Gupta et al. [131] found that HTC increased with increasing velocity, NPs concentration, and heat flux, while the effect of velocity for the same NPs concentration was small. The maximum HTC enhancement was about 78% for the highest NPs concentration and heat flux. Mangrulkar et al. [132] determined an optimum concentration of NPs for which HTC achieved a maximum increase of 52% to 60% depending on the type of NPs. Solangi et al. [133] observed a significant increase in both HTC and Nu number with increasing NPs concentration and heat flux with a maximum of 119% and 85%, respectively. Noghrehabadi and Pourrajab [134] observed an increase in HTC with NPs concentration increase with a maximum of about 23%. The intensification was particularly noticeable in the entrance region. Because the correlation equations for the base fluid incorrectly predicted the obtained HTC, a dedicated correlation equation was proposed—see Table 2. Saxena et al. [135] tested the influence of NPs concentration, mass flow rate, and heat flux on heat transfer during laminar, transition, and turbulent flow. It was established that the maximum HTC rise was 62% and for turbulent flow. It was also shown that an increase in the heat flux for the same mass flow rate and NPs concentration led to a significant increase in HTC. It was suggested that the use of nanofluids was more efficient for turbulent than transition flow. A correlation equation was also proposed—see Table 2. Azmi et al. [136] recorded Nu number increase with NPs concentration and inlet temperature increase with a maximum of about 29%. A correlation equation for transition and turbulent flow was developed—see Table 3. Martínez-Cuenca et al. [137] established that HTC increased significantly as the concentration of NPs increased. For ceramic NPs, the HTC increase was even 84% at high Re numbers. For carbon-based NPs, the increase in HTC reached 48%. Singh et al. [138] observed HTC increase with NPs concentration increase with a maximum of about 45%. A correlation equation for laminar flow was developed—see Table 2. Selvam et al. [139] established a significant increase, as much as 170%, in HTC and 96% increase in Nu number for the maximum tested NPs concentration and for turbulent flow. These results confirmed earlier study by Selvam et al. [129]. Ranjbarzadeh et al. [140] found that for the same Re number, HTC increased with the increase in NPs concentration with a maximum of about 40% for smaller tested Re numbers under turbulent flow. Azmi et al. [141] investigated the effect of water content in the water–EG base fluid mixture and found that the maximum HTC enhancement was for the mixture with the highest water content. For maximum inlet temperature and the highest tested NPs concentration, the maximum HTC increase was about 25% under turbulent flow condition. A correlation equation for various base fluid mixtures for turbulent flow was developed—see Table 3. İlhan and Ertürk et al. [142] found that the maximum increase in HTC of about 15% was similar to the increase in thermal conductivity of nanofluid. Furthermore, the change in Nu number was practically immeasurable in the tested range of parameters. Jumpholkul et al. [143] recorded that Nu number increased with NPs concentration and inlet temperature increase with a maximum of about 35%. A correlation equation generalizing the research results was also proposed—see Table 3. Sundararaj et al. [144] found that the Nu number and HTC coefficient significantly increased with the increase in NPs concentration, and for the maximum tested concentration and the highest Re number, the HTC increase was about 16.3% and for turbulent flow. Cieśliński and Kozak [145] observed a decrease in the Nu number with increasing concentration of NPs up to 25% for the same Re number. Ho et al. [146] observed no increase in the Nu number compared to base fluid with a significant increase in the concentration of NPs. Singh et al. [147] recorded enhancement of HTC with NPs concentration increase up to 24%.

A correlation equation was proposed for laminar flow—see Table 2. Singh et al. [148] found an increase in HTC with NPs concentration increase up to 25%. A correlation equation for two base fluid mixtures was proposed for laminar flow—see Table 2. Solangi et al. [149] established that the Nu number for turbulent flow of nanofluid increased by 54% and 84% for lower and higher examined heat flux, respectively. Singh et al. [150] found that the HTC increased with increasing concentration of NPs, with a maximum of about 40% for laminar flow. Nikulin et al. [151] observed that for the same Re number, the HTC for nanofluids increased with the increase in the concentration of NPs, both for laminar and turbulent flow. However, when the same product of the mass flow rate and specific heat was used as a comparative criterion, it turned out that the addition of NPs had no effect on HTC in laminar flow, while for turbulent flow it caused deterioration of heat transfer. Karabulut et al. [152] found that for turbulent flow, the HTC increased with increasing NPs of concentration up to 48%. Kong and Lee [153] found that HTC increased by about 19% compared to base fluid for the same Re number and maximum NPs concentration and inlet temperature for turbulent flow. Demirkir and Ertürk [154] studied laminar, transition, and early turbulent flow of nanofluids. It was established that the NPs concentration did not affect the local Nu number for the same Re number and distance from the inlet, while the local HTC increased with NPs concentration increase to about 22%. The maximum increase in the average HTC was about 36%. Like Sharma et al. [60], Asirvatham et al. [69], Meyer et al. [88], Wusiman et al. [94], Selvam et al. [129], and Saxena et al. [135], Demirkir and Ertürk [154] observed that the transition from laminar to turbulent flow occurred at lower Re number with NPs concentration increase. Ebaid et al. [155] observed an almost 17% increase in the Nu number with an increase in NPs concentration compared to base fluid for turbulent flow. Siddiqi et al. [156] determined that for the same concentration of NPs, the average HTC decreased from a maximum of about 29% by more than half with a doubling of the tube diameter.

A more detailed summary of the literature results discussed above is presented in Table 1.

Table 1. Review of experimental studies inside straight, round tubes.

Executor	Nanofluid	NPC/d_p [nm]	Surfactant	Geometry	Heating Method	Re
Pak and Cho [40]	Water–Al_2O_3 Water–TiO_2	1–3%vol. $13 \leq d_p \leq 27$	No	D = 10.66 mm L = 4800 mm	SS; q = const. Resistively heated (DC)	10^4–10^5
Li and Xuan [41]	Water–Cu	0.3–2%vol. $d_p < 100$	FAS	D = 10 mm L = 800 mm	brass; q = const. Resistively heated (DC)	800–2.5×10^4
Xuan and Li [42]	Water–Cu	0.3–2%vol. $d_p < 100$	SL	D = 10 mm L = 800 mm	brass; q = const. Resistively heated (DC)	10^4–2.5×10^4
Wen and Ding [43]	Water–Al_2O_3	0.6–1.6%vol. $27 \leq d_p \leq 56$	SDBS	D = 4.5 mm L = 970 mm	Cu; q = const. Silicone rubber heater	500–2100
Yang et al. [44]	ATF–graphite SO–graphite	2–2.5%wt. $1 \leq d_{av}$ [μm] ≤ 2 $20 \leq \delta_p$ [nm] ≤ 40	No	D = 4.57 mm L = 457 mm	Double tube	5–110
Kabelac and Kuhnke [45]	Water–Al_2O_3 EG–Al_2O_3	0.5–1%vol. 1%vol. d_p = 28	No	D = 8 mm L = 500 mm D = 0.7 mm L = 500 mm	Cu; t_w = const. Steam condensation	Up to 3×10^4
Heris et al. [46]	Water–Al_2O_3 Water–CuO	0.2–3%vol. d_p = 20 $50 \leq d_p \leq 60$	No	D = 6 mm L = 1000 mm	Cu; t_w = const. Steam condensation	650–2050
Heris et al. [47]	Water–CuO	0.2–3%vol. $50 \leq d_p \leq 60$	No	D = 6 mm L = 1000 mm	Cu; t_w = const. Steam condensation	650–2050
Ding et al. [48]	Water–MWCNT	0.1–0.5%wt. l/d > 100	SDBS AG SL	D = 4.5 mm L = 970 mm	Cu; q = const. Silicone rubber heater	800–1200
Heris et al. [49]	Water–Al_2O_3	0.2–2.5%vol. d_p = 20	No	D = 6 mm L = 1000 mm	Cu; t_w = const. Steam condensation	700–2050
Williams et al. [50]	Water–Al_2O_3 Water–ZrO_2	0.9–3.6%vol. d_p = 46 0.2–0.9%vol. d_p = 60	No	D = 9.4 mm L = 2820 mm	SS; q = const. Resistively heated (DC)	9×10^3–63×10^3
Kulkarni et al. [51]	Water/EG(40/60)–SiO_2	2–10%vol. $20 \leq d_p \leq 100$	No	D = 3.14 mm L = 1000 mm	Cu; q = const. Strip heaters	3×10^3–12×10^3

Table 1. *Cont.*

Executor	Nanofluid	NPC/d_p [nm]	Surfactant	Geometry	Heating Method	Re
Sommers and Yerkes [52]	Propanol–Al_2O_3	0.5–3%wt $d_p = 10 \pm 5$	Yes–P	D = 19.05 mm L = 457.2 mm	Double tube	500–5500
Kim et al. [53]	Water–Al_2O_3 Water–carbonic	3–3.5%vol. $20 \leq d_p \leq 50$ $d_p = 20$	No	D = 4.57 mm L = 2000 mm	SS; q = const. Resistively heated (DC)	800–6500
Anoop et al. [54]	Water–Al_2O_3	1–6%wt $45 \leq d_p \leq 150$	No	D = 4.75 mm L = 1200 mm	Cu; q = const. Heater wire	500–2000
Yu et al. [55]	Water–SiC	3.7%vol. $d_p = 170$	No	D = 2.27 mm L = 580 mm	SS; q = const. Resistively heated (DC)	3.3×10^3–13×10^3
Liao and Liu [56]	Water–MWCNT	0.5–2%wt $1 \leq l\,[\mu m] \leq 2$ $10 \leq d \leq 20$	No	D = 1.02 mm L = 221 mm	SS; q = const Resistively heated	500–10^4
Hwang et al. [57]	Water–Al_2O_3	0.01–0.3%vol. $d_p = 30 \pm 5$	No	D = 1.812 mm L = 2500 mm	SS; q = const Resistively heated (AC)	390–800
Asirvatham et al. [58]	Water–CuO	0.003%vol. $d_p = 40$	No	D = 8 mm L = 1500 mm	Cu; q = const Heating tape	1350–2170
Tori and Yang [59]	Water–ND	0.1–1%vol. $2 \leq d_p \leq 10$	No	D = 4 mm L = 1000 mm	SS; q = const Resistively heated (DC)	3×10^3–6×10^3
Sharma et al. [60]	Water–Al_2O_3	0.02–0.1%vol. $d_p = 47$	SDBS	D = 19 mm L = 1500 mm	Cu; q = const. Heater wire	3.5×10^3–8.5×10^3
Duangthongsuk and Wongwises [61]	Water–TiO_2	0.2–2%vol. $d_p = 21$	No	D = 8.13 mm L = 1500 mm	Double tube	3×10^3–18×10^3
Mosavian et al. [62]	Water–Al_2O_3 Water–CuO Water–Cu	0.2–3%vol. $d_p = 20$ 0.2–3%vol. $d_p = 50$ 0.2–2.5%vol. $d_p = 25$	No	D = 6 mm L = 1000 mm	Cu; t_w = const. Steam condensation	600–2000
Fotukian and Esfahany [63]	Water–Al_2O_3	0.2%vol. $d_p = 20$	No	D = 5 mm L = 1000 mm	Cu; t_w = const. Steam condensation	6×10^3–31×10^3

Table 1. *Cont.*

Executor	Nanofluid	NPC/d_p [nm]	Surfactant	Geometry	Heating Method	Re
Fotukian and Esfahany [64]	Water–CuO	0.015–0.24%vol. $30 \leq d_p \leq 50$	No	D = 5 mm L = 1000 mm	Cu; t_w = const. Steam condensation	5.2×10^3–31.1×10^3
Vajjha et al. [65]	Water/EG(40/60)–Al_2O_3 Water/EG(40/60)–CuO Water/EG(40/60)–SiO_2	2–10%vol. $d_p = 45$ $d_p = 29$ $20 \leq d_p \leq 100$	No	D = 3.14 mm L = 1168 mm	Cu; q = const. Strip heaters	6×10^3–16×10^3
Amrollahi et al. [66]	Water–MWCNT	0.1–0.25%wt $150 \leq d \leq 200$	No	D = 11.42 mm L = 1000 mm	Cu; q = const Resistively heated (AC)	1600–6×10^3
Xie et al. [67]	Water/EG(55:45)–Al_2O_3 Water/EG(55:45)–TiO_2 Water/EG(55:45)–ZnO Water/EG(55:45)–MgO	0.5–2.5%vol. $10 \leq d_p \leq 60$ $d_p = 30 \pm 5$ $d_p = 30 \pm 5$ $d_p = 30 \pm 5$	ns	D = 2.7 mm	Cu; t_w = const. Cooling bath	150–1500
Baby and Ramaprabhu [68]	Water–graphene EG–graphene	0.005–0.05%vol. ns	No	D = 23 mm L = 1080 mm	SS; q = const Coil (DC)	4.5×10^3–15.5×10^3
Asirvatham et al. [69]	Water–Ag	0.3–0.9%vol. $d_p < 100$	No	D = 4.3 mm L = 2940 mm	Double tube	10^3–11×10^3
Sajadi and Kazemi [70]	Water–TiO_2	0.05–0.25%vol. $d_p = 30$	No	D = 5 mm L = 1200 mm	Cu; t_w = const. Steam condensation	5×10^3–30×10^3
Ferrouillat et al. [71]	Water–SiO_2	5–34%wt 2.3–18.9%vol. $d_p = 22$	No	D = 4 mm L = 500 mm	Double tube	200–10^4
Ho et al. [72]	Water–Al_2O_3	2–10%wt $d_p = 33$	ApH	D = 3.4 mm L = 700 mm	Cu; q = const. Coil (DC)	195–1801
Timofeeva et al. [73]	Water/EG(50:50)–SiC	1–4%vol $16 \leq d_p \leq 90$	ApH	D = 2.27 mm L = 580 mm	SS; q = const. Resistively heated (DC)	4.5×10^3–7.5×10^3
Chandrasekar and Suresh [74]	Water–Al_2O_3	0.1–0.2%vol. $d_p = 43$	No	D = 4.85 mm L = 1200 mm	Cu; q = const. Heater wire	600–7×10^3

Table 1. *Cont.*

Executor	Nanofluid	NPC/d_p [nm]	Surfactant	Geometry	Heating Method	Re
Abdulhassan et al. [75]	Water–Al_2O_3 Water–Al Water–CuO	0.25–2.5%vol. d_p = 30 d_p = 25 d_p = 50	No	D = 4 mm L = 2500 mm	Pyrex, q = const. Coil (AC)	100–900
Shokouhi et al. [76]	Water–Al_2O_3	0.5–1%vol. $20 \leq d_p \leq 30$	SDBS	D = 12.4 mm L = 1460 mm	Cu; t_w = const. Water bath	650–2300
Vishwanadula and Nsofor [77]	Water–Al_2O_3	0.5–4.5%vol. d_p = 45	No	ns	Double tube	9.5×10^3–21×10^3
Heyhat et al. [78]	Water–Al_2O_3	0.1–2%vol. d_p = 40	No	D = 5 mm L = 2000 mm	Cu; t_w = const. Steam condensation	3×10^3–13.5×10^3
Kayhani et al. [79]	Water–TiO_2	0.1–2%vol. d_p = 15	FNPs	D = 5 mm L = 2000 mm	Cu; q = const Coil (DC)	6×10^3–16×10^3
Nine et al. [80]	Water–Al_2O_3	0.5–1.5%vol. $30 \leq d_p \leq 50$	No	D = 4.5 mm L = 1000 mm	Cu; q = const Silicone rubber heater (DC)	300–1100
Yu et al. [81]	Water/EG(55:45) –Al_2O_3	0.01–0.02%vol. d_p = 30	No	D = 2.7 mm	Cu; t_w = const. Cooling bath	100–2×10^3
Julia et al. [82]	Water–Al_2O_3 Water–SiO_2	1–5%vol. d_p = 11 d_p = 12	No	D = 24 mm L = 1000 mm	Al; q = const Band heaters	3×10^3–10^5
Saeedinia et al. [83]	EO–CuO	0.2–2%wt d_p = 50	No	D = 14 mm L = 1200 mm	Cu; q = const Silicone rubber heater (AC)	20–120
Arani and Amani [84]	Water–TiO_2	0.2–2%vol. d_p = 30	CTAB	D = 8.18 mm L = 1288 mm	Double tube	8×10^3–51×10^3
Almohammadi et al. [85]	Water–Al_2O_3	0.5–1%vol. d_p = 15	No	D = 7 mm L = 1000 mm	Cu; q = const Heater wire	500–1500
Kumaresan et al. [86]	Water/EG–MWCNT	0.15–0.45%vol. d< 100	SDBS	D = 10.7mm L = 2500 mm	Double tube	500–5.2×10^3
Azmi et al. [87]	Water–SiO_2	0.5–4%vol. d_p = 22	No	D = 16 mm L = 1500 mm	Cu; q = const Heater wire	5×10^3–27×10^3

Table 1. *Cont.*

Executor	Nanofluid	NPC/d_p [nm]	Surfactant	Geometry	Heating Method	Re
Meyer et al. [88]	Water–MWCNT	0.33–1%vol. $3 \leq d_{in} \leq 5$ $10 \leq d_{out} \leq 20$ $10 \leq l\,[\mu m] \leq 30$	AG	D = 5.16 mm L = 1000 mm	Cu; q = const Coil heater (DC)	10^3–8×10^3
Ferrouillat et al. [89]	Water–SiO_2 (spherical) Water–SiO_2 (rod) Water–ZnO (polygonal) Water–ZnO (rod-like shape)	2.5%wt. ≡ 1.08%vol. ns 4%wt. ≡ 2.28%vol. ns 4.4%wt. ≡ 0.82%vol. ns 5%wt. ≡ 0.93%vol. ns	FNPs	D = 4 mm L = 500 mm	Double tube Cooling mode Heating mode	200–15×10^3
Abreu et al. [90]	Water–MWCNT	0.25–0.5%vol. $50 \leq d_{out} \leq 80$ $10 \leq l\,[\mu m] \leq 20$	FNPs	D = 6 mm L = 1200 mm	SS, q = const Silicone rubber heater (DC)	1240–2060
Haghighi et al. [91]	Water–Al_2O_3 Water–TiO_2 Water–CeO_2	9%wt. $d_p = 10$ $20 \leq d_p \leq 30$ $50 \leq d_p \leq 100$	PACSS PAAS	D = 0.5 mm L = 300 mm	SS, q = const Resistively heated (DC)	380–1050
Paul et al. [92]	Ionic liquid–Al_2O_3 Spherical/whiskers	0.5%wt $d_p < 50$	No	D = 3.86 mm L = 990.6 mm	SS, q = const Heating tape (DC)	583–2193
Sahin et al. [93]	Water–Al_2O_3	0.5–4%vol. ns	No	D = 11.7 mm L = 770 mm	Al; q = const Heating tape	4×10^3–20×10^3
Wusiman et al. [94]	Water–Cu	0.1–1%vol. $d_p = 50$	No	D = 4.5 mm L = 1000 mm	Cu, q = const Heater wire (AC)	300–16×10^3
Heyhat et al. [95]	Water–Al_2O_3	0.1–2%vol. $d_p = 40$	No	D = 5 mm L = 2000 mm	t_w = const. Steam condensation	330–2100
Feng and Li [96]	EG–SiO_2 Water/EG(50:50)–SiO_2	0.2–2%vol. $15 \leq d_p \leq 50$		D = 10 mm L = 900 mm	Cu; q = const Resistively heated (DC)	9–450
Rayatzadeh et al. [97]	Water–TiO_2	0.1–0.25%vol. $d_p = 30$	CTAB	D = 4.2 mm L = 2740 mm	Cu; q = const Heater wire	850–1950

Table 1. *Cont.*

Executor	Nanofluid	NPC/d_p [nm]	Surfactant	Geometry	Heating Method	Re
Esmaeilzadeh et al. [98]	Water–Al_2O_3	0.5–1%vol. d_p = 15	No	D = 7 mm L = 1000 mm	Cu; q = const Heater wire	300–2 × 10^3
Meriläinen et al. [99]	Water–Al_2O_3 Water–SiO_2 Water–MgO	0.5–4%vol. $d_p = 8.2 \pm 3.1$ $14 \leq d_p \leq 53$ $d_p = 6.5 \pm 1.8$ $d_p = 65 \pm 34$ $14 \leq d_p \leq 53$ $d_p = 21 \pm 10$ $15 \leq d_p \leq 47$	ApH	D = 7 mm L = 1500 mm	t_w = const. Steam condensation	3 × 10^3–10^4
Azmi et al. [100]	Water–TiO_2 Water–SiO_2	0.5–3%vol. d_p = 50 d_p = 22	No	D = 16 mm L = 1500 mm	Cu, q = const Heater wire	5 × 10^3–25 × 10^3
Gupta et al. [101]	Water–TiO_2	0.05–0.5%wt $30 \leq d_p \leq 50$	No	D = 8 mm L = 1050 mm	Cu, q = const Heater wire	1663–2433
Mojarrad et al. [102]	Water/EG(50:50)–Al_2O_3	0–0.7%vol. $20 \leq d_p \leq 30$	SDBS	D = 12.4 mm L = 1460 mm	Cu; t_w = const. Heating bath	650–2300
Chiney et al. [103]	Water–Al_2O_3 EG–Al_2O_3 Water/EG(50:50)–Al_2O_3	0.5–1.25%vol. $80 \leq d_{p,50} \leq 95$	Yes—ns	D = 6 mm L = 520 mm	Double tube	Laminar
Haghighi et al. [104]	Water–Al_2O_3 Water-TiO_2 Water–ZrO_2	9%wt d_p = 68 d_p = 300 d_p =237	Yes—ns PAAS PAAS	D = 3.7 mm L = 1500 mm	Double tube	100–9 × 10^3
Sadeghinezhad et al. [105]	Water–GNP	0.025–0.1%wt. d_{av} = 2 µm δ = 2 nm	No	D = 10 mm L = 1400 mm SS, q = const	SS, q = const Heating tape (DC)	5 × 10^3–22 × 10^3
Ghozatloo et al. [106]	Water–GNS	0.05–0.1%wt. ns	AOM with KPS	D = 10.7 mm L = 1000 mm	Cu; q = const. Heater wire	1940
Halelfadl et al. [107]	Water–MWCNT	0.05%wt. ≡ 0.026%vol $d_{out} \approx$ 9.2 nm l = 1.5 µm	Lignin SP	D = 18.7 mm L = 660 mm	Double tube	500–2050

Table 1. *Cont.*

Executor	Nanofluid	NPC/d_p [nm]	Surfactant	Geometry	Heating Method	Re
Reddy and Rao [108]	Water/EG(60:40)–TiO_2	0.0004–0.02%vol. d_p = 21	No	D = 8.13 mm L = 1500 mm	Double tube	4×10^3–15×10^3
Ho and Lin [109]	Water–Al_2O_3	2–10%wt ≡ 0.56–2.98%vol. d_p = 33	No	D = 3.4 mm L = 700 mm	Cu; q = const. Coil (DC)	3×10^3–13×10^3
Utomo et al. [110]	Water–Al_2O_3 Water–TiO_2 Water–CNT	9%wt ≡ 2.4%vol. $100 \leq d_p \leq 200$ $10 \leq d_p \leq 20$ $20 \leq d_p \leq 50$ 0.3%wt ≡ 0.14%vol. $20 \leq d_{out} \leq 40$ $10 \leq l\ [\mu m] \leq 20$	PVP	D = 4.57 mm L = 1220 mm	SS; q = const. Coil (DC)	400–2200
	Water–Al_2O_3 Water–TiO_2 Water–CNT	9%wt ≡ 0.2.4%vol. $100 \leq d_p \leq 200$ $10 \leq d_p \leq 20$ $20 \leq d_p \leq 50$ 0.3%wt ≡ 0.14%vol. $20 \leq d_{out} \leq 40$ $10 \leq l\ [\mu m] \leq 20$	PVP	D = 3.7 mm L = 1468 mm	SS; q = const. Resistively heated (DC)	400–2200
Esfe et al. [111]	Water–MgO	0.0625–1%vol. d_p = 40	CTAB	L = 1110 mm	Double tube	3.2×10^3–19×10^3
Akhavan-Zanjani et al. [112]	Water–graphene	0.005–0.02%vol. $0.4 \leq \delta \leq 1.3$ nm 270 nm × 1.5 μm	PVA	D = 4.2 mm	Cu; q = const. Heater wire (AC)	5×10^3–11×10^3
Sahin et al. [113]	Water–CuO	0.5–4%vol. d_p = 33	CTAB SDBS	D = 11.7 mm L = 770 mm	Al; q = const Heating tape	4×10^3–20×10^3
Akhavan-Behabadi et al. [114]	HTO–CuO	0.5–1.5%wt. d_p = 40	No	D = 8.62 mm L = 500 mm	t_w = const. Steam condensation	200–750
Mehrali et al. [115]	Water–GNP	0.025–0.1%wt d_{av} = 2 μm δ = 2 nm	No	D = 4.5 mm L = 1404 mm	SS; q = const. Resistively heated (DC)	290–2300

Table 1. *Cont.*

Executor	Nanofluid	NPC/d_p [nm]	Surfactant	Geometry	Heating Method	Re
Amiri et al. [116]	TO–MWCNT	0.001–0.1%vol. $d_{out} \leq 30$ $5 \leq l\ [\mu m] \leq 15$	HA	L = 1300 mm	Cu; q = const. Electrical resistances	300–1000
Colla et al. [117]	Water–TiO_2	1–2.5%wt 0.6 nm $\leq d_p \leq$ 6 µm	AA	D = 8 mm L = 2000 mm	Cu; q = const. Heater wire	400–1600
Minakov et al. [118]	Water–CuO	0.25–2%vol. d_p = 55	XGP	D = 4 mm L = 1000 mm	Cu; q = const. Heater wire	50–3500
Sadeghinezhad et al. [119]	Water–GNP	0.025–0.1%wt ns	No	D = 10 mm L = 1400 mm	SS; q = const. Heating tape	4.6×10^3–18.2×10^3
Chavan and Pise [120]	Water–Al_2O_3	0.1–1%vol. d_p = 30	No	D = 10.6 mm L = 1000 mm	Cu; t_w = const. Heating bath	6×10^3–14×10^3
Usri et al. [121]	Water/EG(60:40)–Al_2O_3	0.2–0.6%vol. d_p = 13	No	D = 16 mm L = 1500 mm	Cu, q = const Heater wire	2.5×10^3–18×10^3
Cabaleiro et al. [122]	Water/EG(50:50) –ZnO	1%wt. 40 $\leq d_p \leq$ 100	No	D = 8 mm L = 2000 mm	Cu, q = const Heater wire	800–3×10^3
Gómez et al. [123]	Water–CNT	0.12–0.24%vol. 15 $\leq d_{out} \leq$ 30 8 $\leq l\ [\mu m] \leq$ 36	No	D = 6.34 mm L = 2460 mm	Brass; q = const. Heating tape	3×10^3–20×10^3
Patel and Subhedar [124]	Water/EG(50/50)–Al_2O_3	0.2–0.6%vol. d_p = 20	No	D = 10 mm L = 1000 mm	Cu; q = const. Coil heater	Laminar
Esfe et al. [125]	Water–Ag	0.125–1%vol. 30 $\leq d_p \leq$ 50	No	L = 1110 mm	Double tube	3.1×10^3–31×10^3
Akhavan-Zanjani et al. [126]	Water–graphene	0.005–0.02%vol. 0.4 $\leq \delta \leq$ 1.3 nm 270 nm × 1.5 µm	PVA	D = 4.2 mm L = 2740.2 mm	Cu; q = const Heater wire (AC)	600–1900
Hatwar and Kriplani [127]	Water–Al_2O_3 Water–CuO	0.1–0.7%vol. d_p = 45 d_p = 45	No	D = 9.5 mm L = 1000 mm	Cu; q = const Heater wire (AC)	2.8×10^3–5×10^3
Hekmatipour et al. [128]	HTO–CuO	0.5–1.5%wt. d_p = 40	No	D = 8.62 mm L = 500 mm	t_w = const. Steam condensation	113–730

Table 1. *Cont.*

Executor	Nanofluid	NPC/d_p [nm]	Surfactant	Geometry	Heating Method	Re
Selvam et al. [129]	Water/EG(70/30)–Ag	0.05–0.45%vol. $d_p < 100$	SDS	D = 4.3 mm L = 2970 mm	Double tube	500–12.5 × 10^3
Zarringhalam et al. [130]	Water–CuO	0.0625–2%vol. $d_p = 40$	No	L = 1110 mm	Double tube	2.9 × 10^3–18.5 × 10^3
Gupta et al. [131]	Water–MWCNT	0.05–0.5%wt $7 \leq d_{out} \leq 20$ $75 \leq l$ [nm] ≤ 88	No	D = 8 mm L = 1050 mm	Cu; q = const. Heater wire (DC)	1300–2300
Mangrulkar et al. [132]	Water–Al_2O_3 Water–CuO	0.3–0.7%vol. $d_p = 20$ $d_p = 30$	No	D = 9.52 mm L = 800 mm	Cu; q = const. Heater wire (AC)	500–2750
Solangi et al. [133]	PG–Water–GNP	0.025–0.1%wt ns	FGNP	D = 4 mm L = 1500 mm	Cu; q = const. Heating tape	3.9 × 10^3–11.7 × 10^3
Noghrehabadi and Pourrajab [134]	Water–Al_2O_3	0.1–0.9%vol. $d_p = 20$	No	D = 11.1 mm L = 2380 mm	Cu; q = const. Heater wire (AC)	1057–2070
Saxena et al. [135]	Water–Al_2O_3	0.1–0.5%vol. $d_p = 40$	No	D = 11.7 mm L = 1400 mm	Cu; q = const. Heater wire	1500–6 × 10^3
Azmi et al. [136]	Water/EG(60/40)–TiO_2	0.5–1.5%vol. $d_p = 50$	No	D = 16 mm L = 1500 mm	Cu, q = const Heater wire	4 × 10^3–22 × 10^3
Martínez-Cuenca et al. [137]	Water–Al_2O_3 Water–SiO_2 Water–MWCNT	1–5%vol. $d_p = 127$ 1–5%vol. $d_p = 201$ 0.125–1%vol. $d_{out} = 30$ l = 1.5 mm	ApH SDS	D = 24 mm L = 1000 mm	Al; q = const Band heaters	5 × 10^3–10^5
Singh et al. [138]	Water/PG(40:60)–CuO	0.25–1%vol. $d_p = 33$	No	D = 9.96 mm D = 12.9 mm D = 19.24 mm	Double tube	750–1600

Table 1. *Cont.*

Executor	Nanofluid	NPC/d_p [nm]	Surfactant	Geometry	Heating Method	Re
Selvam et al. [139]	Water/EG(30/70)–GNP	0.1–0.5%vol. d_{av} = 15 µm $5 \leq \delta \leq 10$	SD	D = 4.3 mm L = 2970 mm	Double tube	10^3–11×10^3
Ranjbarzadeh et al. [140]	Water–GO	0.025–0.1%vol. d_{av} = 2 µm $3.4 \leq \delta \leq 7$ nm	FGO	D = 8.5 mm	t_w = const. Steam condensation	5.2×10^3–36.5×10^3
Azmi et al. [141]	Water/EG(60/40)–Al_2O_3 Water/EG(50/50)–Al_2O_3 Water/EG(40/60)–Al_2O_3	0.2–1%vol. d_p = 13	No	D = 16 mm L = 1500 mm	Cu; q = const. Heater wire	3×10^3–25×10^3
İlhan and Ertürk [142]	Water–hBN	0.1–1%vol. $60 \leq d_{av} \leq 80$	PVP	D = 6 mm L = 2000 mm	Cu; q = const. Heater wire (AC)	800–1700
Jumpholkul et al. [143]	Water–SiO_2	0.5–2%vol. d_p = 7	No	D = 7 mm L = 2000 mm	SS; q = const. Resistively heated (DC)	3.8×10^3–12×10^3
Sundararaj et al. [144]	Kerosene–Al_2O_3	0.01–0.05%vol. $32 \leq d_p \leq 50$	No	D = 4 mm L = 1000 mm	Cu; q = const. Heater wire	500–5.5×10^3
Cieśliński and Kozak [145]	Water/EG(60/40)–Al_2O_3 Water/EG(50/50)–Al_2O_3	0.1–1%wt $d_p < 50$	No	D = 8 mm L = 2000 mm	SS; q = const. Resistively heated (AC)	3×10^3–8×10^3
Ho et al. [146]	Water–Al_2O_3	10%wt $22.2 \leq d_p \leq 47.7$	No	D = 3.4 mm L = 800 mm	Cu; q = const. Coil (DC)	189–2087
Singh et al. [147]	Water/PG(40:60)–MgO	0.3–0.66%vol. d_p = 22	No	D = 9.96 mm D = 12.9 mm L = 1600 mm	Double tube	1100–2050
Singh et al. [148]	Water/EG(40:60)–Al_2O_3 Water/PG(40:60)–Al_2O_3	1–2.5%vol. 0.6–1.5%vol. $19 \leq d_p \leq 59$	No	D = 9.96 mm D = 12.9 mm D = 19.24 mm	Double tube	1000–3250
Solangi et al. [149]	Water–GNP	0.025–0.1%wt ns	FGNP	D = 4 mm L = 1500 mm	Cu; q = const. Heating tape	3.9×10^3–11.7×10^3

Table 1. *Cont.*

Executor	Nanofluid	NPC/d_p [nm]	Surfactant	Geometry	Heating Method	Re
Singh et al. [150]	Water/PG(40/60)–CuO	0.3–0.7%vol. d_p = 38	Yes—ns	D = 13 mm	Double tube	750–1600
Nikulin et al. [151]	Isopropanol–Al_2O_3	0.387–4.71%wt d_p < 50	No	D = 3.5 mm L = 2400 mm	SS; q = const. Resistively heated	200–8 × 10^3
Karabulut et al. [152]	Water–GO	0.01–0.02%vol. ns	No	D = 8 mm L = 1830 mm	Cu; q = const. Heater wire	2371–3167
Kong and Lee [153]	Water–Al_2O_3	0.38–1.3%vol. d_p = 30	No	D = 12.573 mm L = 1200 mm	Cu; q = const. Heater wire (AC)	5.3 × 10^3–19.5 × 10^3
Demirkir and Ertürk [154]	Water–graphene	0.025–0.2%vol. $5 \leq \delta \leq 10$ nm $5 < l\,[\mu m] < 10$	PVP	D = 6 mm L = 2100 mm	Cu; q = const. Heater wire	1.4 × 10^3–4 × 10^3
Ebaid et al. [155]	Water–Fe_3O_4	0.3–1.2%wt d_p = 10.3	NH_4OH Ethanol	D = 11 mm L = 1200 mm	Cu; q = const. Heater wire	2.2 × 10^3–9.2 × 10^3
Siddiqi et al. [156]	Water–ZnO	0.012–0.048%wt d_p = 20	No	D = 1 mm D = 2 mm L = 330 mm	SS; q = const. Resistively heated (DC)	Laminar

Table 2. Empirical correlation equations for laminar flow of nanofluids.

Authors	Correlation	Nanofluid	Range
Li and Xuan [41]	$\overline{Nu} = 0.4328\left(1.0 + 11.285\varphi^{0.754}Pe_{d_p}^{0.218}\right)Re^{0.333}Pr^{0.4}$	Water–Cu	800 < Re < 2200 0.3%vol < φ < 2%vol
Anoop et al. [54]	$Nu = 4.36 + \left[6.219 \times 10^{-3}x_*^{-1.1522}\left(1 + \varphi^{0.1533}\exp^{(-2.5228x_*)}\right)\right]\left[1 + 0.57825\left(\frac{d_p}{d_{ref}}\right)^{-0.2183}\right]$ $d_{ref} = 100$ nm; $x_* = \frac{x}{DRePr}$	Water–Al_2O_3	500 < Re < 2000 50 < x/D < 200 1%wt < φ < 6%wt
Asirvatham et al. [58]	$Nu = 0.155Re^{0.59}Pr^{0.35}(D/x)^{0.38}$	Water–CuO	1350 < Re < 2170 φ = 0.003%vol D = 8 mm
Chandrasekar and Suresh [74]	$\overline{Nu} = 0.556Pe^{0.348}(1+\varphi)^{181.43}$ $\overline{Nu} = 9.4 \times 10^{-5}Re^{1.42}Pr^{0.4}(1+\varphi)^{371.5}$	Water–Al_2O_3	600 < Re < 7 × 10^3 0.1%vol < φ < 0.2%vol

Table 2. *Cont.*

Authors	Correlation	Nanofluid	Range
Esmaeilzadeh et al. [98]	$Nu = 4.36 + 0.8437\left[0.2315(x_*)^{-0.4991}\left(1+\varphi^{0.123}e^{(-23.53x_*)}\right)\right]$ $x_* = \frac{x}{DRePr}$	Water–Al_2O_3	$300 < Re < 2 \times 10^3$ 0.5%vol < φ < 1%vol
Gupta et al. [101]	$\overline{Nu} = 0.00414Re^{0.55}Pr^{2.1}$	Water–TiO_2	1663 < Re < 2433 0.05%wt < φ < 0.5%wt
Mojarrad et al. [102]	$\overline{Nu} = 0.1899Re^{0.37}Pr^{0.496}\varphi^{0.67}$	Water/EG(1:1) –Al_2O_3 Water–Al_2O_3	650 < Re < 2300 Pr > 4 φ < 0.7%vol
Hekmatipour et al. [128]	$Nu_{nf} = Nu_{bf}\left\{0.68\left(\frac{\mu_{bf}}{\mu_{nf}}\right)^{0.14}(1+\varphi)^{1.6}\left[1+\left(\frac{Gr}{Re^2}\right)^{0.3}\right]^{0.5}\right\}$ $Nu_{bf} = 2.67\left[Gz_{bf}^2 + 0.0087^2(GrPr)^{1.5}\right]^{1/6}$ $Gz = \frac{D}{L}RePr$—Graetz number	HTO–CuO	113 < Re < 730 215 < Pr < 233 7700 < Gr < 32,000 0.5%vol < φ < 1.5%vol
Noghrehabadi and Pourrajab [134]	$Nu = 4.36 + \left(3+\varphi^{0.442}\right)Re^{0.288}Pr^{0.0185}(D/x)^{0.3851}$	Water–Al_2O_3	900 < Re < 2100 0.1%vol < φ < 0.9%vol 40 < x/D < 180
Saxena et al. [135]	$\overline{Nu} = 0.309Re^{0.451}(1+100\varphi)^{0.455}W_{in}^{0.203}$ W_{in}—electrical heating power	Water–Al_2O_3	1500 < Re < 6000 0%vol < φ < 0.5%vol
Singh et al. [138]	$\overline{Nu} = 1.86Pe^{1/3}\left[1+1.87\left(\frac{\varphi}{1-\varphi}\right)^{0.45}\right]$	Water/PG(40/60) –CuO	750 < Re < 1600 $8 \times 10^3 < Pe < 123 \times 10^3$ 0.3%vol < φ < 0.7%vol.
Singh et al. [147]	$\overline{Nu} = 1.86Pe^{1/3}\left[1+4.90\left(\frac{\varphi}{1-\varphi}\right)^{0.576}\right]$	Water/PG(40:60) –MgO	1100 < Re < 2050 $4 \times 10^3 < Pe < 111.4 \times 10^3$ 0.3%vol < φ < 0.66%vol
Singh et al. [148]	$\overline{Nu} = 1.86Pe^{1/3}\left[1+2.536\left(\frac{\varphi}{1-\varphi}\right)^{0.622}\right]$	Water/EG(40:60) –Al_2O_3 Water/PG(40:60) –Al_2O_3	1000 < Re < 3250 $48.5 \times 10^3 < Pe < 83 \times 10^3$ 0.3%vol < φ < 0.66%vol
Singh et al. [157]	$\overline{Nu} = 1.86\left(Pe\frac{D}{L}\right)^{1/3}\left(\frac{\mu}{\mu_w}\right)^{0.14}\left[1+0.316(\varphi A)^{0.208}\right]$ A ≈ 6 for Water-EG based nanofluids A ≈ 11 for Water-PG based nanofluids	Water/PG–CuO Water/PG–MgO Water/EG–Al_2O_3 Water/PG–Al_2O_3	Laminar flow 0.3%vol < φ < 0.7%vol.

Table 3. Empirical correlation equations for transition and turbulent flow of nanofluids.

Authors	Correlation	Nanofluid	Range
Pak and Cho [40]	$\overline{Nu} = 0.021Re^{0.8}Pr^{0.5}$	Water–Al_2O_3 Water–TiO_2	$10^4 < Re < 10^5$ $6.5 < Pr < 12.3$ $1\%vol < \varphi < 3\%vol$
Li and Xuan [41]	$\overline{Nu} = 0.0059\left(1.0 + 7.6286\varphi^{0.6886}Pe_{d_p}^{0.001}\right)Re^{0.9238}Pr^{0.4}$	Water–Cu	$10^4 < Re < 2.5 \times 10^3$
Sharma et al. [60]	$\overline{Nu} = 3.13 \times 10^{-3}RePr^{0.6}(1+\varphi)^{1.22}$	Water–Al_2O_3	$3.5 \times 10^3 < Re < 8.5 \times 10^3$ $4.5 < Pr < 5.5$ $35 < t\,[^\circ C] < 40$ $0.02\%vol < \varphi < 0.1\%vol$
Vajjha et al. [65]	$\overline{Nu} = 0.065(Re^{0.65} - 60.22)(1 + 0.0169\varphi^{0.15})Pr^{0.542}$	Water/EG–Al_2O_3 Water/EG–CuO Water/EG–SiO_2	$3 \times 10^3 < Re < 16 \times 10^3$ $\varphi < 10\%vol$–Al_2O_3 $\varphi < 6\%vol$–CuO, SiO_2
Sajadi and Kazemi [70]	$\overline{Nu} = 0.067Re^{0.71}Pr^{0.35} + 0005Re$	Water–TiO_2	$5 \times 10^3 < Re < 30 \times 10^3$ $\varphi \leq 0.25\%vol$
Chandrasekar and Suresh [74]	$\overline{Nu} = 0.556Pe^{0.348}(1+\varphi)^{181.43}$ $\overline{Nu} = 9.4 \times 10^{-5}Re^{1.42}Pr^{0.4}(1+\varphi)^{371.5}$	Water–Al_2O_3	$600 < Re < 7 \times 10^3$ $0.1\%vol < \varphi < 0.2\%vol.$
Vishwanadula and Nsofor [77]	$\overline{Nu} = 1.752Re^{1.618}Pr^{-8.819}$	Water–Al_2O_3	$9.5 \times 10^3 < Re < 21 \times 10^3$ $0.5\%vol < \varphi < 4.5\%vol$
Arani and Amani [84]	$\overline{Nu} = 0.041Re^{0.83}Pr^{1.35}\left(1+\varphi^{0.43}\right)$	Water–TiO_2	$8 \times 10^3 < Re < 51 \times 10^3$ $0.2\%vol < \varphi < 2\%vol$
Azmi et al. [87]	$\overline{Nu} = 0.00896Re^{0.7406}Pr_w^{1/3}(f_r/8)^{-3.606}(0.1+\varphi/100)^{2.541}$ $f_r = \frac{f_{nf}}{f_B} = \left[\left(\frac{\rho_{nf}}{\rho_w}\right)^{1.3}\left(\frac{\mu_{nf}}{\mu_w}\right)^{0.3}\right]$ and $f_B = 0.3164Re^{-0.25}$	Water–SiO_2	$5 \times 10^3 < Re < 27 \times 10^3$ $0.5\%vol < \varphi < 4\%vol$
Sahin [93]	$\overline{Nu} = 0.106Re^{0.588}Pr^{0.258}\left(1+\varphi^{-0.1096}\right)$	Water–Al_2O_3	$4 \times 10^3 < Re < 20 \times 10^3$ $5 < Pr < 7$ $0.5\%vol < \varphi < 4\%vol$
Esmaeilzadeh et al. [98]	$Nu = 4.36 + 0.8437\left[0.2315(x_*)^{-0.4991}\left(1+\varphi^{0.123}e^{(-23.53x_*)}\right)\right]$ $x_* = \frac{x}{DRePr}$	Water–Al_2O_3	$300 < Re < 2 \times 10^3$ $0.5\%vol < \varphi < 1\%vol$
Chavan and Pise [120]	$\overline{Nu} = 0.508358Re^{0.7401}Pr^{-0.7026}$	Water–Al_2O_3	$6 \times 10^3 < Re < 14 \times 10^3$ $0.3\%vol < \varphi < 1\%vol$

Table 3. *Cont.*

Authors	Correlation	Nanofluid	Range
Saxena et al. [135]	$\overline{Nu} = 0.309Re^{0.451}(1+100\varphi)^{0.455}P^{0.203}$ P—electrical heating power	Water–Al_2O_3	$1.5 \times 10^3 < Re < 6 \times 10^3$ 0%vol < φ < 0.5%vol
Azmi et al. [136]	$\overline{Nu} = Nu_{DB}\left[4.227(1+Pr)^{-0.271}(0.0001+\varphi/100)^{0.1562}\right]$ $\overline{Nu}_{DB} = 0.023Re^{0.8}Pr^{0.4}$	Water/EG(60:40) –TiO_2	$4 \times 10^3 < Re < 22 \times 10^3$ 0.5%vol < φ < 1.5%vol.
Azmi et al. [141]	$\overline{Nu} = 0.025Re^{0.76}Pr^{0.45}\left(1+\frac{T}{70}\right)^{0.14}(0.01+BR)^{-0.1}$ BR—based ratio of water to EG	Water/EG(60/40) –Al_2O_3 Water/EG(50/50) –Al_2O_3 Water/EG(50/50) –Al_2O_3	$3 \times 10^3 < Re < 25 \times 10^3$ 0.2%vol < φ < 1%vol $0.6667 \leq BR \leq 1.6$
Jumpholkul et al. [143]	$\overline{Nu} = 0.001142Re^{1.26}Pr^{-0.19}(1+\varphi)^{14.45}(t_{in}/25)^{-0.4}$	Water–SiO_2	$3.8 \times 10^3 < Re < 12 \times 10^3$ 0.5%vol < φ < 2%vol
Singh et al. [148]	$\overline{Nu} = 1.86Pe^{1/3}\left[1+2.536\left(\frac{\varphi}{1-\varphi}\right)^{0.622}\right]$	Water/EG(40:60) –Al_2O_3 Water/PG(40:60) –Al_2O_3	1000< Re < 3250 48.5×10^3 <Pe< 83×10^3 0.3%vol < φ < 0.66%vol

Table 4. Empirical correlation equations for laminar, transition, and turbulent flow of nanofluids.

Asirvatham et al. [69]	$\overline{Nu} = 0.023Re^{0.8}Pr^{0.3} + (0.617\varphi - 0.135)Re^{(0.445\varphi-0.37)}Pr^{(1.081\varphi-1.305)}$	Water–Ag	$0.8 \times 10^3 < Re < 12 \times 10^3$ 4 < Pr < 10 0%vol < φ < 2%vol

3. Discussion

In this section, a comparison of the measurement results obtained by different research groups for selected water-based nanofluids is presented. Comparisons in graphical form are made for the same tested nanofluids, under the same measurement conditions, in order to answer the fundamental question about the possibility of intensifying heat transfer through a given fluid under specific thermal and flow conditions. Three groups of nanofluids based on ceramic, metallic, and carbonaceous nanoparticles were distinguished.

3.1. Ceramic Nanofluids

This is the most studied category of nanofluids due to the availability of ceramic NPs both in terms of price and quantity. An important feature of ceramic materials is their chemical stability. Ceramic materials include oxides, carbides, and nitrides.

3.1.1. Water–Al_2O_3 Nanofluids

Figure 1 compares available experimental data for water–Al_2O_3 nanofluid in laminar flow in the form of average and local HTC, average and local Nu number as a function of Re number, and dimensionless distance from the tube inlet.

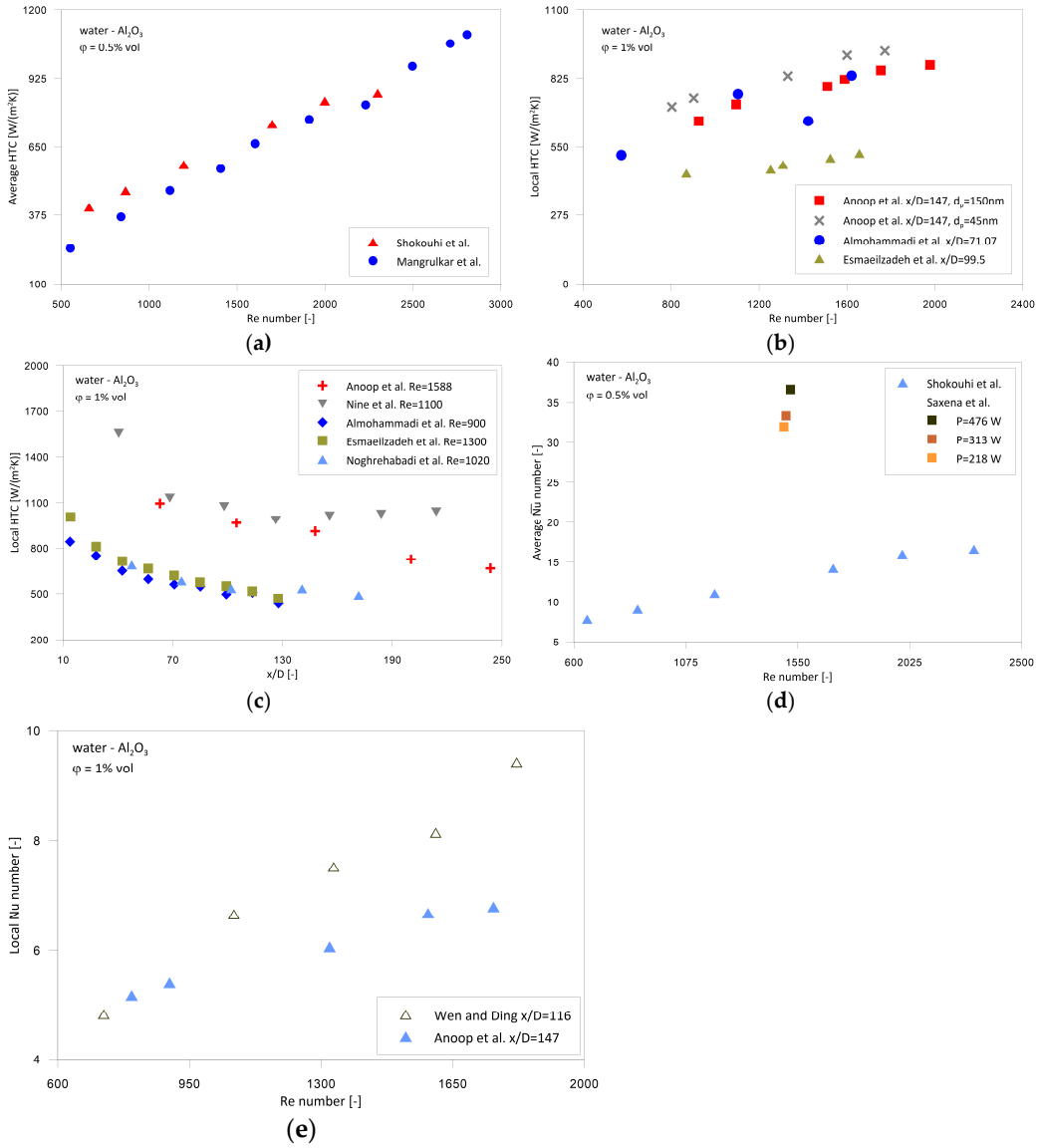

Figure 1. Comparison of water–Al_2O_3 studies during laminar flow: **(a)** $\overline{h} = f(Re)$; **(b)** $h = f(Re)$; **(c)** $h = f(x/D)$; **(d)** $\overline{Nu} = f(Re)$; and **(e)** $Nu = f(Re)$ [43,54,76,80,85,98,132,134,135].

Figure 1a shows the average HTC as a function of the Re number. As shown in Figure 1a, the agreement between the results of Shokouhi et al. [76] and Mangrulkar et al. [132] is very good, even though different thermal boundary conditions were used—see Table 1. Figure 1b shows the dependence of the local HTC as a function of the Re number for the closest possible dimensionless distance from the inlet. Concordance of the results of Anoop et al. [54] and Almohammadi et al. [85] is satisfactory considering the fact that they refer to a significantly different x/D. Local HTC in research by Esmaeilzadeh et al. [98] is much lower than that of Almohammadi et al. [85], although tests were carried out on the same test stand. Lower local HTC for study by Esmaeilzadeh et al. [98] may be due to the fact that they refer to a greater dimensionless distance from the inlet, and it is known that local HTC decreases with increasing x/D [43,48,53,57,80,86,88,92,101,115,126,131,134,144]. Moreover, according to a study by Anoop et al. [54], the smaller the diameter of the NPs, the higher the local HTC. Figure 1c shows the dependence of the local HTC as a function of dimensionless distance from the inlet for the closest possible Re number. As can be seen from Figure 1c, there are clearly two groups of results. In the group of results with about twice as much local HTC, there are studies by Anoop et al. [54] and Nine et al. [80], while in the second group there are studies by Almohammadi et al. [85], Esmaeilzadeh et al. [98], and Noghrehabadi and Pourrajab [134]. The analysis shows that the obtained results do not depend on the boundary condition used in the research. The difference may be due to the diameter of the tube, which in the case of Anoop et al. [54] and Nine et al. [80] was about 56% lower than in the studies by Almohammadi et al. [85] and Esmaeilzadeh et al. [98], and over 144% lower than in the study of Noghrehabadi and Pourrajab [134]. This comparison shows that the smaller the diameter of the tube in the laminar flow of nanofluid, the higher the local HTC. Figure 1d shows the relationship between average Nu number against Re number. As can be seen from Figure 1d, Shokouhi et al. [75] obtained an average Nu number almost three times lower than that of Saxena et al. [135] for a Re number of about 1550 for very similar heater section geometries. It is true that the temperature of the nanofluid at the inlet was, in the study of Saxena et al. [135], higher than in study by Shokouhi et al. [75] by –35 °C and 28 °C, respectively, but this does not explain such a difference in average Nu number. It seems that the reason lies in the measurement procedure used by Shokouhi et al. [75], based on the energy balance, which is extremely sensitive to the temperature measurements. It is worth noting that the results obtained by Saxena et al. [135] for the transition flow—Figure 2c—are similar to those obtained by other researchers, which will be discussed below. Figure 1e illustrates the relationship between local Nu number against Re number for the closest possible dimensionless distance from the inlet. As shown in Figure 1e, the agreement of the results obtained by Wen and Ding [43] and Anoop et al. [54] is very good for the smallest Re numbers. For higher Re numbers, Wen and Ding [43] obtained higher Nu numbers than Anoop et al. [54], which may be due to the fact that in the case of the Wen and Ding study [43], the dimensionless distance from the inlet was lower.

Figure 2 compares available experimental data for water–Al_2O_3 nanofluid in transition flow in the form of average HTC and average Nu number as a function of Re number for various NPs concentrations.

Figure 2a illustrates the relationship of average HTC as a function of Re number. As shown in Figure 2a, the results presented in the literature are very divergent. Fotukian and Esfahany [63] and Heyhat et al. [78] conducted tests for the same diameter of the tube and using the same measurement procedure. The higher local HTC obtained by Fotukian and Esfahany [63] compared to Heyhat et al. [78] can be explained by a slightly higher concentration of NPs, −0.135% vol and 0.1% vol, respectively. The HTC values obtained by Hatwar and Kriplani [127] are significantly lower than those of Fotukian and Esfahany [63] and Heyhat et al. [78], which may result from the applied calculation method based on the energy balance. Figure 2b illustrates the relationship of average HTC as a function of Re number for higher NPs concentration. As shown in Figure 2b, the average HTC obtained by Haghighi et al. [104] is much higher than in the study of Heyhat et al. [78], which may be due to the very small diameter of the tube used in the tests (3.7 mm). The very well-

documented measurements seem to justify the extremely high HTC obtained by Haghighi et al. [104], bearing in mind that they relate to single-phase convection. Figure 2c illustrates the relationship of average Nu number as a function of Re number. As shown in Figure 2c, the average Nu number obtained by Sharma et al. [60], Fotukian and Esfahany [63], and Saxena et al. [135] shows good agreement both qualitatively and quantitatively, despite different diameters of the tested tubes and different measurement techniques. It is worth noting the increase in the Nu number with the increase in the electrical heating power, which was shown by Saxena et al. [135]. Figure 2d illustrates the relationship of average Nu number as a function of Re number for higher NPs concentration. As shown in Figure 2d, the average Nu number obtained by Chavan and Pise [120] is higher than in the study of Kong and Lee [153], which may be due to much higher temperatures of the nanofluid at the inlet, i.e., 20–40 °C, compared to 10–30 °C in the study by Kong and Lee [153]. It is worth noting the increase in the Nu number with the increase in Pr number, which was shown by Kong and Lee [153].

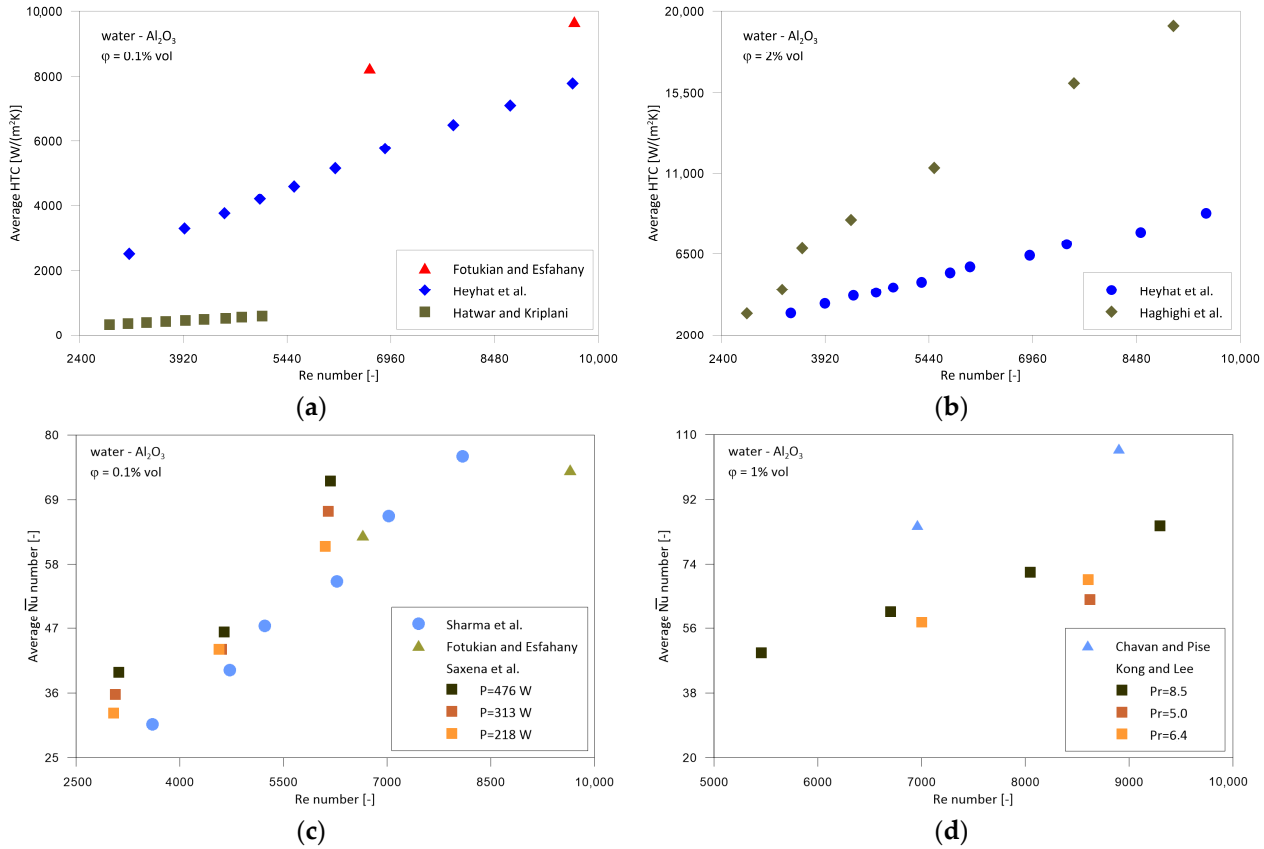

Figure 2. Comparison of water–Al_2O_3 studies during transition flow: (**a**) $\overline{h} = f(Re)$; (**b**) $\overline{h} = f(Re)$; (**c**) $\overline{Nu} = f(Re)$; and (**d**) $\overline{Nu} = f(Re)$ [60,63,78,91,120,127,135,153].

Figure 3 compares available experimental data for water–Al_2O_3 nanofluid in turbulent flow in the form of average HTC and average Nu number as a function of Re number for the same NPs concentration.

As shown in Figure 3a, the average HTC obtained by Julia et al. [82] is significantly lower than in the studies of Pak and Cho [40], Heyhat et al. [78], Sahin et al. [93], and Chavan and Pise [120]. There seem to be several reasons why HTC is so different. Julia et al. [120] used an unusual heating section, i.e., tube with a large internal diameter (31.2 mm) and thick wall (3.6 mm), and that was relatively short (L/D = 32). Moreover, the used NPs with an initial diameter of 11 nm tended to strongly agglomerate. As a result, the real average diameter of the agglomerates was 127 nm, and the maximum agglomerate diameter was as much as 218 nm. Therefore, the deposition of such large particles on the wall of the

tube cannot be ruled out, which leads to the creation of additional thermal resistance and explains the lower HTC compared to other tests.

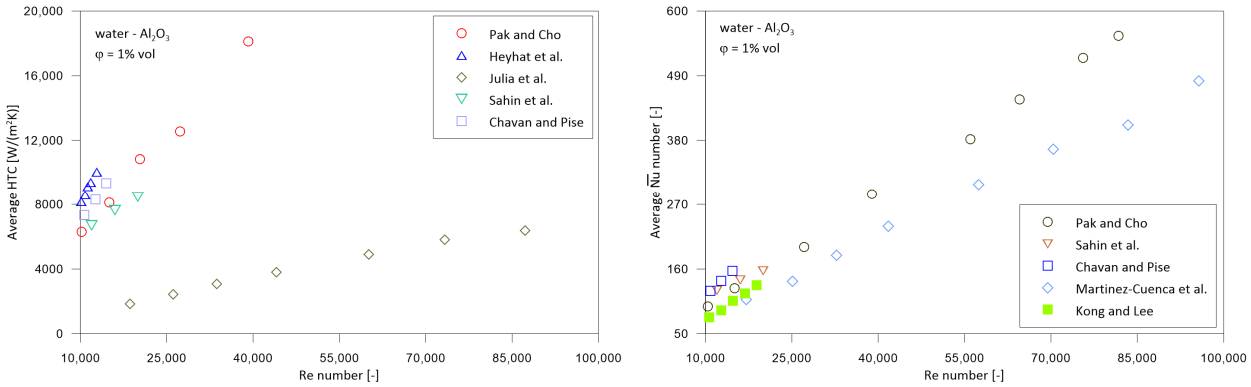

Figure 3. Comparison of water–Al_2O_3 studies during turbulent flow: (**a**) $\overline{h} = f(Re)$; and (**b**) $\overline{Nu} = f(Re)$ [40,78,82,93,120,137,153].

As shown in Figure 3b, the average Nu number obtained by Pak and Cho [40], Sahin et al. [93], Chavan and Pise [120], Martinez-Cuenca et al. [137], and Kong and Lee [153] show very good agreement for the early range of turbulent flow, i.e., lower Re numbers. For Re numbers higher than 19,000, only the results of Pak and Cho [40] and Martinez-Cuenca et al. [137] can be compared, whereby Pak and Cho [40] obtained a higher average Nu number than Martinez-Cuenca et al. [137], which may be due to the smaller diameter of the tube used in the study.

3.1.2. Water–TiO_2 Nanofluids

Figure 4 compares available experimental data for water–TiO_2 nanofluid in laminar flow in the form of local Nu number as a function of dimensionless distance from the inlet for the same Re number.

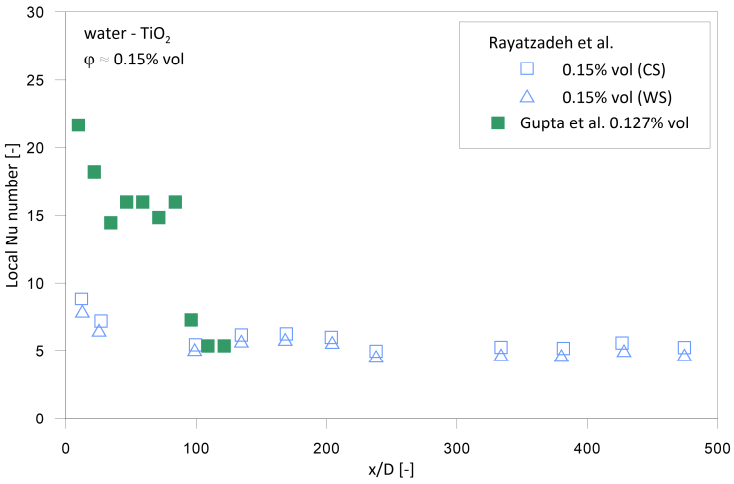

Figure 4. Comparison of $Nu = f(x/D)$ distribution for water–TiO_2 nanofluid during laminar flow [97,101].

As shown in Figure 4, the local Nu number obtained by Rayatzadeh et al. [97] and Gupta et al. [101] shows very good agreement for the dimensionless distance from the inlet higher than x/D > 100. For x/D < 100, i.e., for a region with a developing boundary layer of high heat transfer intensity, Gupta et al. [101] obtained a much higher local Nu number than Rayatzadeh et al. [97], which may result from sedimentation of NPs. It is worth noting

the positive influence of continuous sonication (CS) on local Nu number, which was shown by Rayatzadeh et al. [97].

Figure 5 compares available experimental data for water–TiO_2 nanofluid in transition flow in the form of average HTC and average Nu number as a function of Re number for various NPs concentrations.

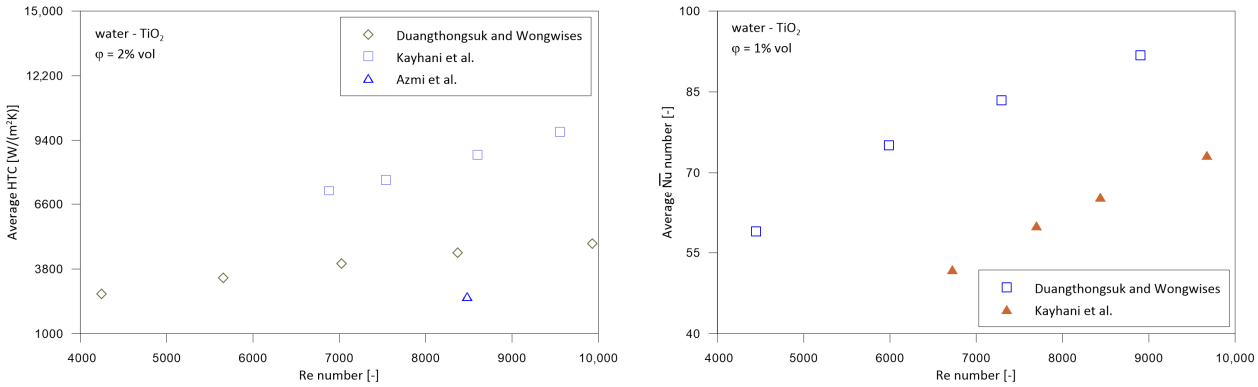

Figure 5. Comparison of water–TiO_2 studies during transition flow: (**a**) $\overline{h} = f(Re)$; and (**b**) $\overline{Nu} = f(Re)$ [61,79,100].

As shown in Figure 5a, Kayhani et al. [79] recorded much higher average HTC than Duangthongsuk and Wongwises [61] and Azmi et al. [100], which may result from the use of NPs with a very small diameter—15 nm, which were additionally functionalized, thus protected against agglomeration. Duangthongsuk and Wongwises [61] and Azmi et al. [100] used in their research NPs with primary diameters of 21 nm and 30–50 nm, respectively. In addition, no surfactants were used to stabilize the fabricated nanofluids.

As shown in Figure 5b, the relationship between average Nu number in the studies of Kayhani et al. [79] and Duangthongsuk and Wongwises [61] is quite different than the relationship between average HTC presented in Figure 5a. For average Nu number, Duangthongsuk and Wongwises [61] obtained much higher values than Kayhani et al. [79], contrary to the average HTC. The main difference between the results shown in Figure 5a,b results from the fact that they present data for different concentrations of NPs. In their research, Duangthongsuk and Wongwises [61] determined that there is an optimum concentration of NPs, which for water–TiO_2 nanofluids in transition flow is 1%vol.

Figure 6 compares available experimental data for water–TiO_2 nanofluid for turbulent flow in the form of average HTC and average Nu number as a function of Re number for various NPs concentrations.

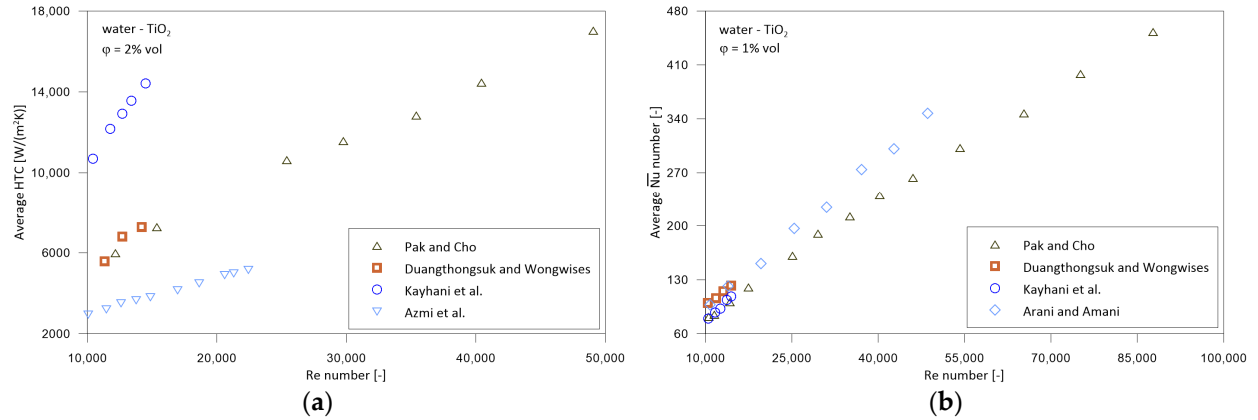

Figure 6. Comparison of water–TiO_2 studies during turbulent flow: (**a**) $\overline{h} = f(Re)$; and (**b**) $\overline{Nu} = f(Re)$ [40,61,79,84,100].

As shown in Figure 6a, the average HTC for turbulent flow of water–TiO_2 nanofluid is very divergent. It is clear that the results of Kayhani et al. [79] significantly differ from those obtained by Pak and Cho [40], Duangthongsuk and Wongwises [61], and Azmi et al. [100], which are basically the same. It should be emphasized that for an NPs concentration of 2%vol, Pak and Cho [40], Duangthongsuk and Wongwises [61], and Azmi et al. [100] observed a decrease in the average HTC compared to the base fluid (water), while Kayhani et al. [79] determined an increase in the average HTC compared to the base fluid for this NPs concentration. It is significant that in the case of the average Nu number for the concentration of NPs equal to 1%vol, the results of Kayhani et al. [79] do not differ from other researchers—see Figure 6b.

3.1.3. Water–SiO_2 Nanofluids

Figure 7 compares available experimental data for water–SiO_2 nanofluid in transition flow in the form of average HTC and average Nu number as a function of Re number for various NPs concentrations.

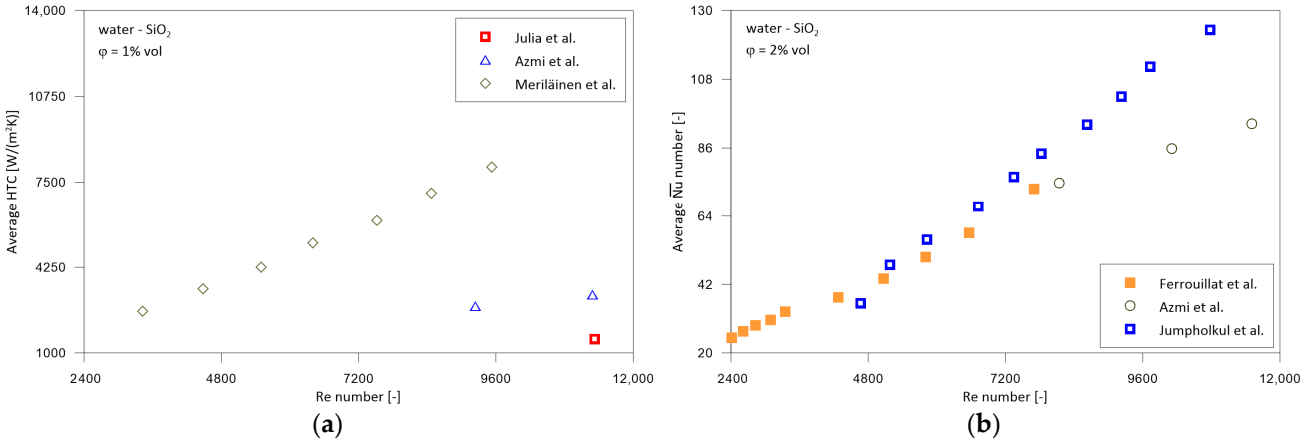

Figure 7. Comparison of water–SiO_2 studies during transition flow: (**a**) $\overline{h} = f(Re)$; and (**b**) $\overline{Nu} = f(Re)$ [71,82,87,99,143].

As shown in Figure 7a, the average HTC for transition flow of water–SiO_2 nanofluid is very divergent. The results of Meriläinen et al. [99] are significantly higher than those obtained by Azmi et al. [87] and Julia et al. [82], which are convergent. According to Meriläinen et al. [99], the decisive factor in heat transfer enhancement is the average size of NPs. As already discussed above, NPs in the Julia et al. study [120] showed a tendency to form agglomerates with dimensions above 200 nm. Contrary to average HTC results, the $\overline{Nu} = f(Re)$ relationship obtained in research by Ferrouillat et al. [71], Azmi et al. [87], and Jumpholkul et al. [143] are very consistent—see Figure 7b.

Figure 8 compares available experimental data for water–SiO_2 nanofluid in turbulent flow in the form of average HTC and average Nu number as a function of Re number for the same NPs concentration.

As shown in Figure 8a, Azmi et al. [87] obtained a much higher average HTC than Julia et al. [82], although they carried out measurements at a much lower temperature of the nanofluid. The bulk temperature in [87] was 30 °C while in [82] the inlet temperature was 60 °C. It seems that the reason for the much lower HTC in the study of Julia et al. [82] was the agglomeration of NPs and their deposition on the surface of the tube, which resulted in an increase in thermal resistance. The comparison of the $\overline{Nu} = f(Re)$ relationship for turbulent flow was possible only for the early range of Re number, because no one except Martinez-Cuenca et al. [137],conducted research for such large Re numbers. As shown in Figure 8b, results achieved by Jumpholkul et al. [143] show very good agreement with the research of Martinez-Cuenca et al. [137].

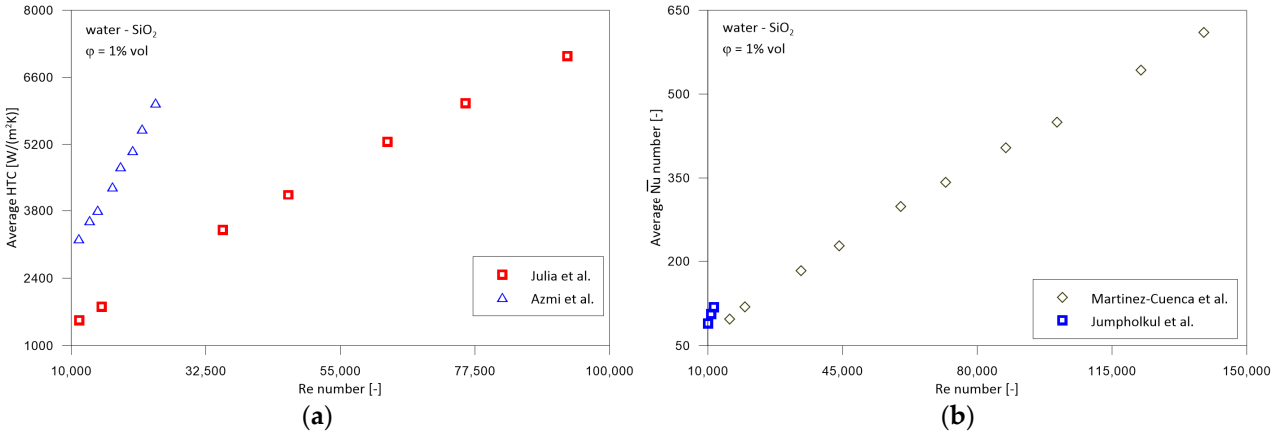

Figure 8. Comparison of water–SiO_2 studies during turbulent flow: (**a**) $\overline{h} = f(Re)$; and (**b**) $\overline{Nu} = f(Re)$ [82,87,137,143].

3.1.4. Water–CuO Nanofluids

Figure 9 compares available experimental data for water–CuO nanofluid in laminar flow in the form of average HTC as a function of Re number.

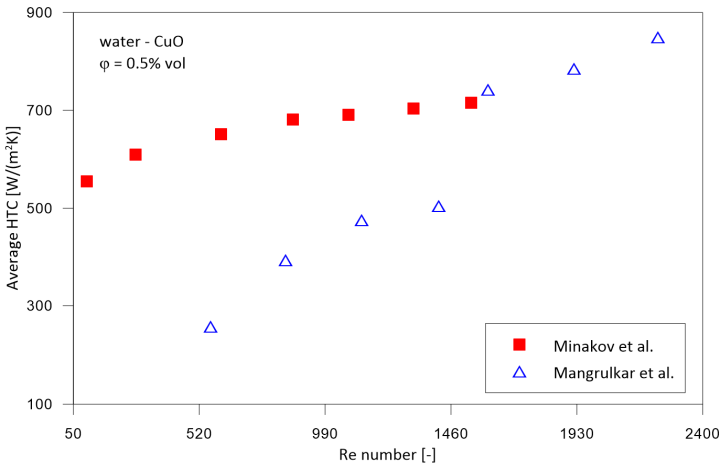

Figure 9. Comparison of $\overline{h} = f(Re)$ relationship for water–CuO studies during laminar flow [118,132].

As shown in Figure 9, for Re < 1700, average HTC obtained by Mangrulkar et al. [132] is clearly lower than in the study by Minakov et al. [118]. However, for Re > 1700, the results of Mangrulkar et al. [132] follow the same trend as the data of Minakov et al. [118]. The abrupt increase in average HTC for Re ≈ 1700 in the case of Mangrulkar et al. [132] may result from the change of laminar to transition flow [129].

Figure 10 compares available experimental data for water–CuO nanofluid in transition flow in the form of average HTC and average Nu number as a function of Re number for various NPs concentrations.

As shown in Figure 10a, the average HTC obtained by Fotukian et al. [64] for Re = 8100 is about 28% lower than in the study by Zarringhalam et al. [130]. Bearing in mind that this is a transitional region, this compliance can be considered satisfactory. As shown in Figure 10b, agreement between average Nu number determined by Sahin et al. [113] and Zarringhalam et al. [130] is very good.

Figure 11 compares available experimental data for water–CuO nanofluid in turbulent flow in the form of average HTC and average Nu number as a function of Re number for various NPs concentrations.

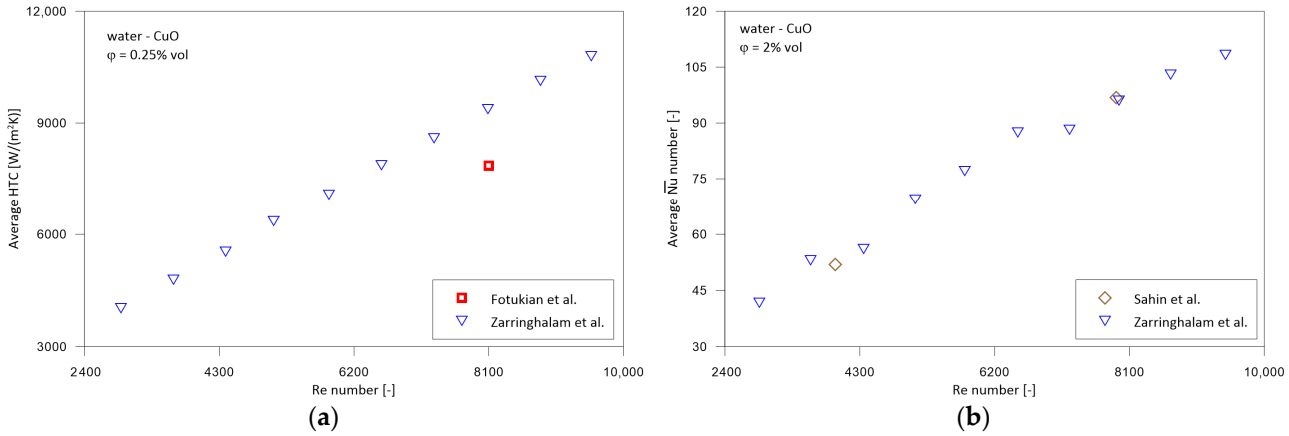

Figure 10. Comparison of water–CuO studies during transition flow: (**a**) $\overline{h} = f(Re)$; and (**b**) $\overline{Nu} = f(Re)$ [64,113,130].

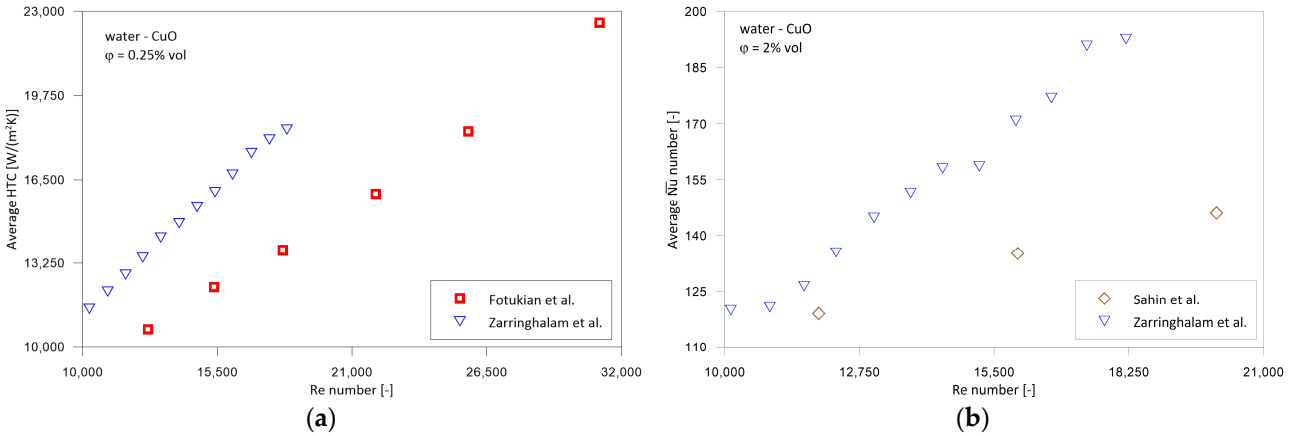

Figure 11. Comparison of water–CuO studies during turbulent flow: (**a**) $\overline{h} = f(Re)$; and (**b**) $\overline{Nu} = f(Re)$ [64,113,130].

As shown in Figure 11a, average HTC obtained by Fotukian et al. [64] and Zarringhalam et al. [130] shows qualitative agreement, however HTC determined by Zarringhalam et al. [130] is about 30% higher in the whole Re number range. The difference in the results of Fotukian et al. [64] and Zarringhalam et al. [130] may result from the method of preparing the nanofluid. Fotukian et al. [64] used sonication for 10 h, while Zarringhalam et al. [130] used sonication for only 3 h. As results from [158–161], sonication time has a significant impact on both the stability of nanofluids and thermophysical properties, such as thermal conductivity and viscosity. As shown in Figure 11b, both Sahin et al. [113] as well as Zarringhalam et al. [130] found that average Nu number increases linearly with Re number increase. However, the $\overline{Nu} = f(Re)$ relationship obtained by Zarringhalam et al. [130] is much steeper than that of Sahin et al. [113], hence, for the highest Re number, i.e., Re $\approx$ 20,000, the average Nu number in the Zarringhalam et al. [130] study is about 45% higher. The difference may result from the use by Sahin et al. [113] of surfactants to improve the stability of the produced nanofluids. As results from [162–166], the application of surfactants can significantly affect the stability and thermophysical properties of nanofluids.

3.2. Metallic Nanofluids

This class of nanofluids is not as often studied as ceramic nanofluids due to cost of precious metal nanoparticles (Ag, Pt) and limited oxidative stability (Al, Cu). The conducted literature research made it possible to carry out a comparison only for the nanofluids containing Cu and Ag nanoparticles.

3.2.1. Water–Ag Nanofluids

Figure 12 compares published experimental data for water–Ag nanofluid in transition and turbulent flow in the form of average Nu number as a function of Re number.

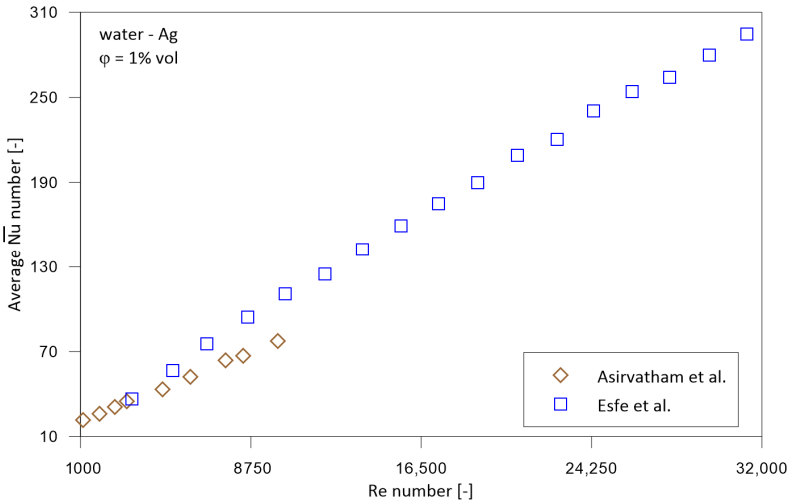

Figure 12. Comparison of $\overline{Nu} = f(Re)$ relationship for water–Ag nanofluids during transition and turbulent flow [69,125].

As shown in Figure 12, results achieved by Asirvatham et al. [69] show very good agreement with the research of Esfe et al. [125].

3.2.2. Water–Cu Nanofluids

Figure 13 compares published experimental data for water–Cu nanofluid in laminar, transition, and turbulent flow.

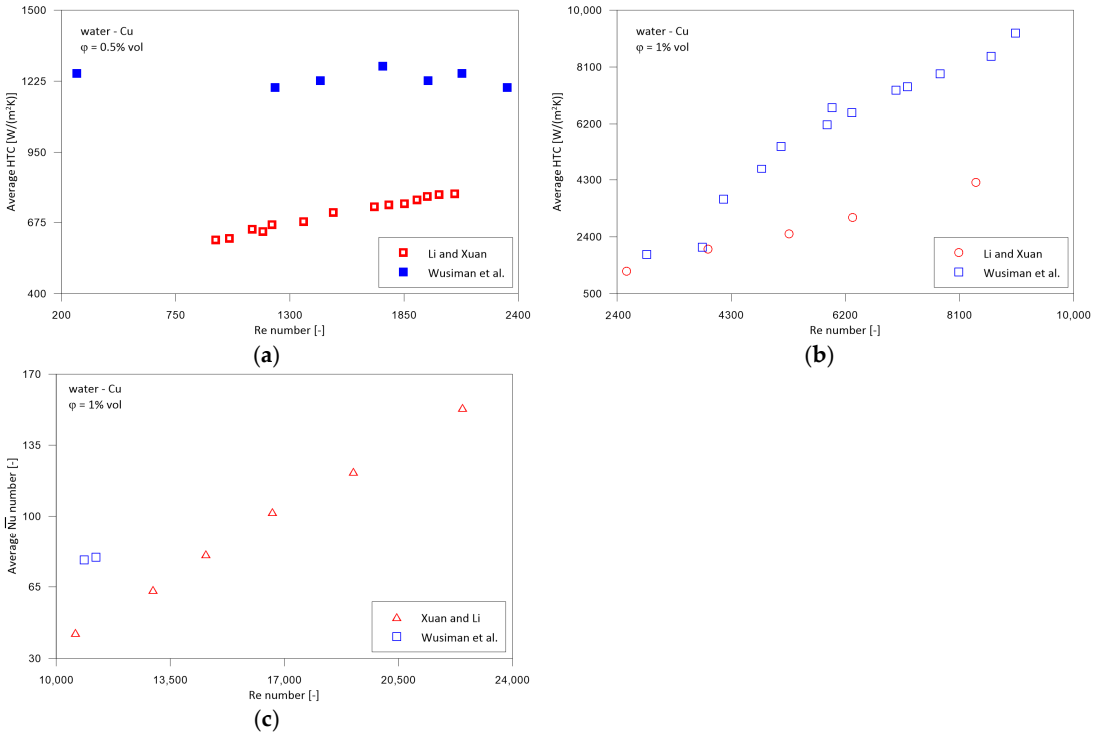

Figure 13. Comparison of the studies for water–Cu nanofluid: (**a**) $\overline{h} = f(Re)$ relationship during laminar flow; (**b**) $\overline{h} = f(Re)$ relationship for transition flow; and (**c**) $\overline{Nu} = f(Re)$ relationship for turbulent flow [41,42,94].

As shown in Figure 13a, average HTC obtained by Wusiman et al. [94] is almost constant against Re number and about two times higher than measured by Li and Xuan [41]. For transition flow and higher NPs concentration, the average HTC obtained by Wusiman et al. [94] and Li and Xuan [41] increases linearly with Re number increase; however, the increase in HTC in the Wusiman et al. [94] study is more significant—see Figure 13b. As shown in Figure 13c, the average Nu number obtained by Wusiman et al. [94] is about two times higher than that determined by Xuan and Li [42]. Higher average HTC and average Nu number for studies by Wusiman et al. [94] may result from two reasons—half the diameter of the tested tube and the use of surfactants by Li and Xuan [41] and Xuan and Li [42], respectively, which could adversely change the thermophysical properties of the produced nanofluids.

3.3. Carbonaceous Nanofluids

This category of nanofluids raises high hopes due to the excellent thermal conductivity of carbon-based nanoparticles, such as graphite, graphene, CNT, etc.

3.3.1. Water–MWCNT Nanofluids

Despite numerous works in which the water–MWCNT nanofluid was used [48,56,66, 88,90,107,131,137], due to significant discrepancies in the concentration of NPs, as well as the tested range of the Re number, only the results of two studies could be compared.

Figure 14 compares published experimental data for water–MWCNT nanofluid in laminar and transition flow in the form of average Nu number as a function of Re number.

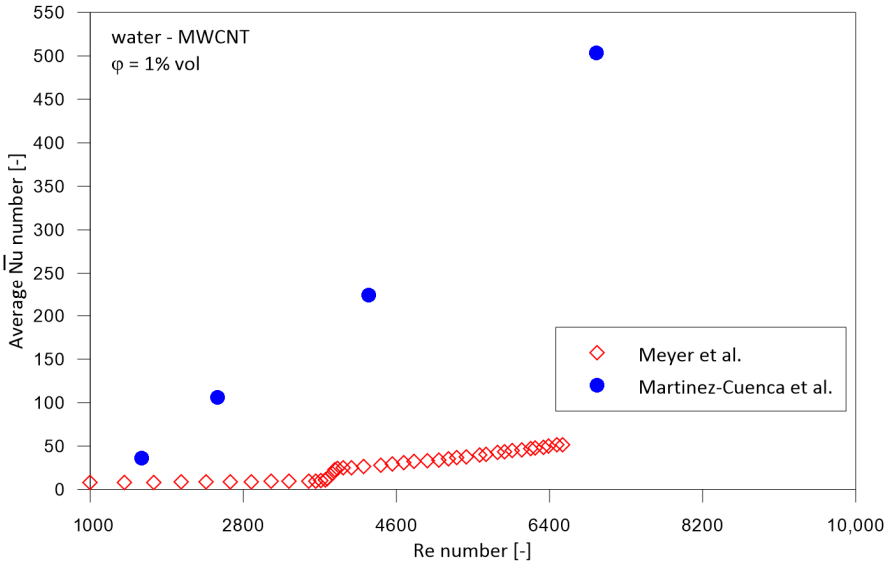

Figure 14. Comparison of $\overline{Nu} = f(Re)$ relationship for water–MWCNT nanofluid during laminar and transition flow [88,137].

As shown in Figure 14, average Nu number obtained by Martinez-Cuenca et al. [137] is about an order of magnitude higher than measured by Meyer et al. [88]. The most likely reason for such low Nu numbers in the Meyer et al. [88] study was the instability of the produced nanofluid, the pH of which was 7.1, while Xie et al. [167] found that the iso-electric point for water–MWCNT(1%vol) is 7.3.

3.3.2. Water–Graphene Nanofluids

Figure 15 compares published experimental data for water–graphene nanofluid in laminar, transition, and turbulent flow.

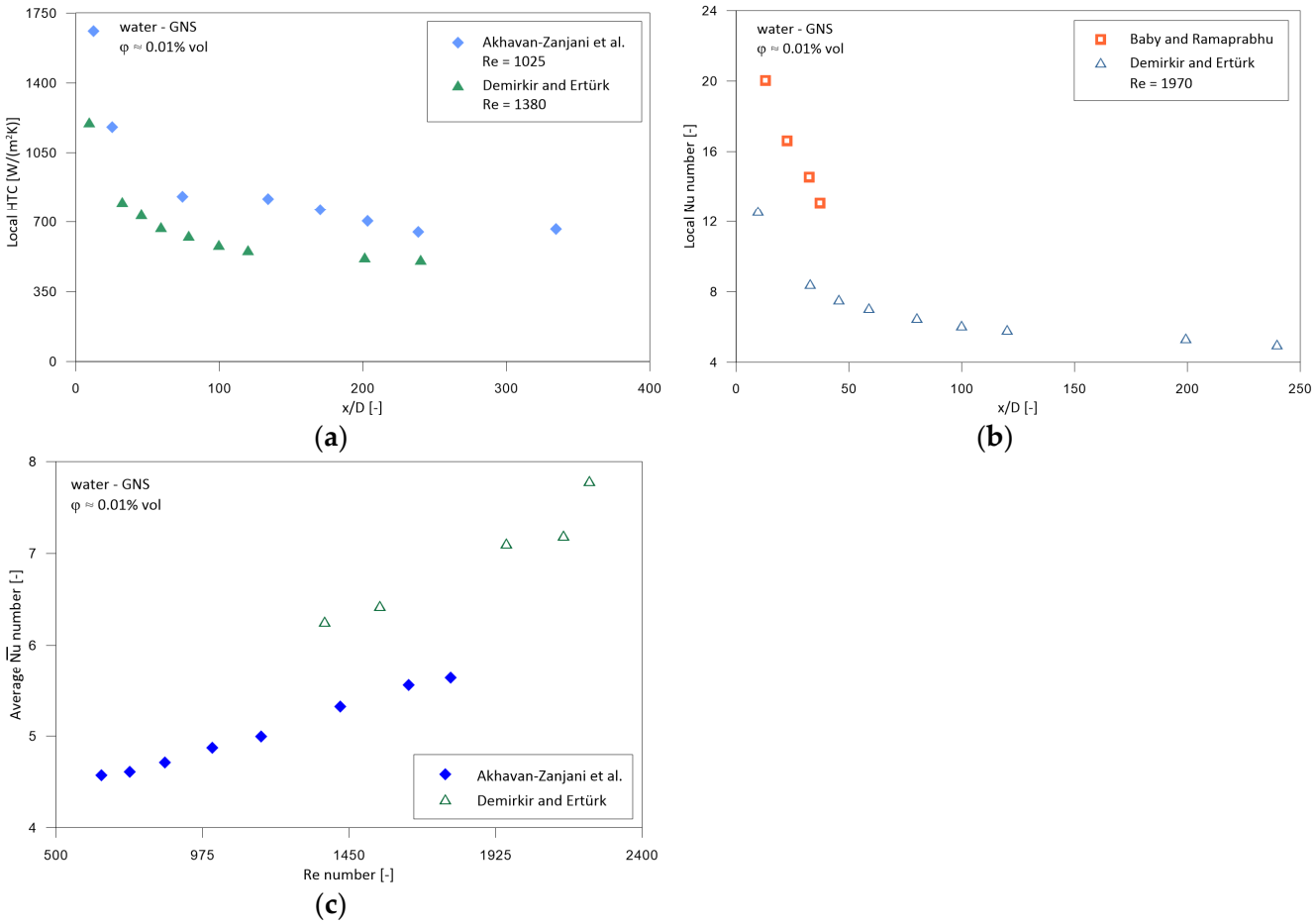

Figure 15. Comparison of the studies for water–graphene nanofluid: (**a**) $\overline{h} = f(x/D)$ relationship for laminar flow; (**b**) $Nu = f(x/D)$ relationship for laminar and transition flow; and (**c**) $\overline{Nu} = f(Re)$ relationship for laminar flow [68,112,154].

As shown in Figure 15a, the change of local HTC against dimensionless distance from the inlet obtained by Akhavan-Zanjani et al. [112] and Demirkir and Ertürk [154] shows good agreement both qualitatively and quantitatively, despite different Re numbers.

As shown in Figure 15b, the local Nu number against dimensionless distance from the inlet obtained by Baby and Ramaprabhu [68] is higher than recorded by Demirkir and Ertürk [154], which results from a much higher Re number in the case of Baby and Ramaprabhu [68]. However, it is worth emphasizing the qualitative consistency of the research results in both cases.

As shown in Figure 15c, average Nu number obtained by Demirkir and Ertürk [154] is about 20% higher than determined by Akhavan-Zanjani et al. [112]. The geometry of the heating section, heating method, and nanofluid preparation were very similar in both cases. However, the graphene structure used in both studies was different. Akhavan-Zanjani et al. [112] determined the thickness of the studied graphene sheets as 0.4–1.3 nm, while Demirkir and Ertürk [154] reported, after the manufacturer, the thickness of the studied graphene nanoplatelets as 5–10 nm, and with a much larger lateral size, i.e., 5–10 µm, compared to 270 nm–1.5 µm in the study by Akhavan-Zanjani et al. [112].

3.3.3. Water–GNP Nanofluids

Figure 16 compares published experimental data for water–GNP nanofluid in transition and turbulent flow in the form of average Nu number as a function of Re number.

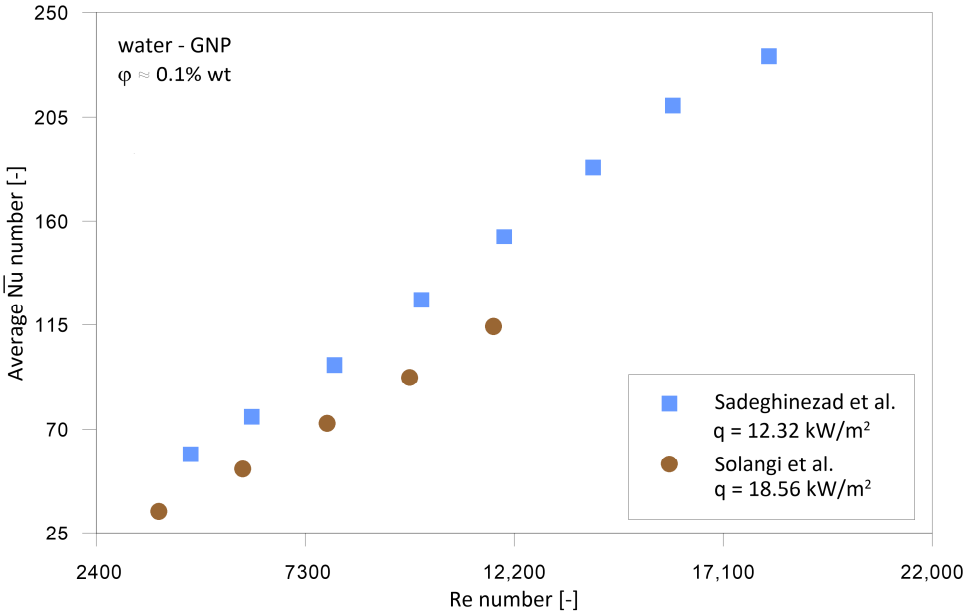

Figure 16. Comparison of $\overline{Nu} = f(Re)$ relationship for water–GNP nanofluid during transition and turbulent flow [119,133].

As shown in Figure 16, the $\overline{Nu} = f(Re)$ relationship obtained by Sadeghinezhad et al. [119] and Solangi et al. [133] is linear with the maximum discrepancy between both studies of about 40% for turbulent flow. The higher Nu number achieved by Sadeghinezhad et al. [119], despite the lower heat flux, may result from the higher purity of the GNP used. In the case of Sadeghinezhad et al. [119], the carbon content was greater than 99.5%, while in the study of Solangi et al. [133], it was about 95%.

3.4. Nanofluids with Different Base Fluids

In this subsection, a comparison of the measurement results obtained by different research groups for different nanofluids is presented. Comparisons in graphical form are made for the same type of nanoparticles but different base fluids, under the same flow conditions, in order to find the answer to which of the base fluids is the most favorable for the same thermal and flow conditions.

Figure 17 compares available experimental data for Al_2O_3 nanoparticles of different NPs concentration in laminar flow in the form of average HTC as a function of Re number.

As shown in Figure 17a, Yu et al. [81] obtained for water–EG(55/45)–Al_2O_3 nanofluid higher average HTC than that determined by Sundararaj et al. [144] for kerosene–Al_2O_3 nanofluid for very low NPs concentration and the same Re number. Figure 17b shows that average HTC obtained by Shokouhi et al. [76] and Mangrulkar et al. [132] for water–Al_2O_3 nanofluid was higher than that determined by Mojarrad et al. [102] for water–EG(50/50)–Al_2O_3 nanofluid. Contrary to Shokouhi et al. [76] and Mangrulkar et al. [132], Mojarrad et al. [102] established lower average HTC for water–Al_2O_3 nanofluid than that for water–EG(50/50)–Al_2O_3 nanofluid. Figure 17c shows that for laminar flow, regardless of the inlet temperature, average HTC determined by Nikulin et al. [151] for the isopropanol–Al_2O_3 nanofluid was lower than that for water–Al_2O_3 nanofluid determined by Shokouhi et al. [76]. For Re > 1940, average HTC for isopropanol–Al_2O_3 nanofluid was higher than for water–Al_2O_3, which results from the change of the flow regime from laminar to transition, while the flow of water–Al_2O_3 nanofluid was still laminar.

Figure 18 compares available experimental data for Al_2O_3 nanoparticles of different NPs concentrations in transition–turbulent flow in the form of average HTC as a function of Re number and average Nu number as a function of Re number.

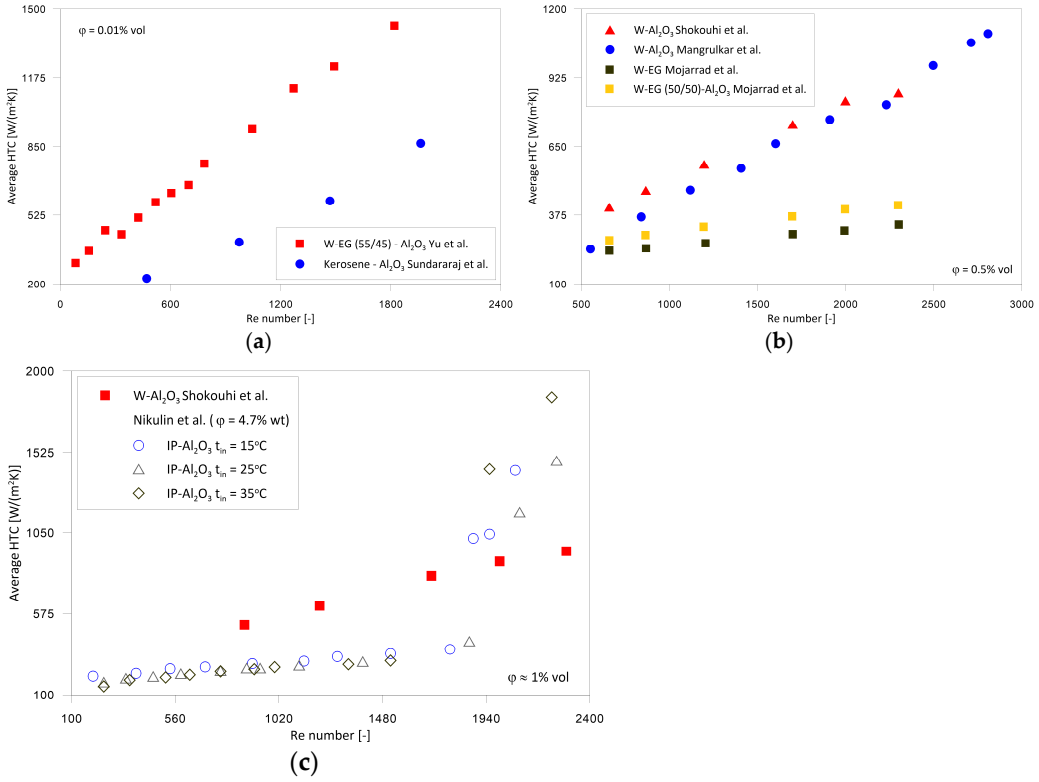

Figure 17. Comparison of different base fluid–Al_2O_3 studies during laminar flow: (**a**) $\overline{h} = f(Re)$; (**b**) $\overline{h} = f(Re)$; and (**c**) $\overline{h} = f(Re)$ [76,81,102,132,144,151].

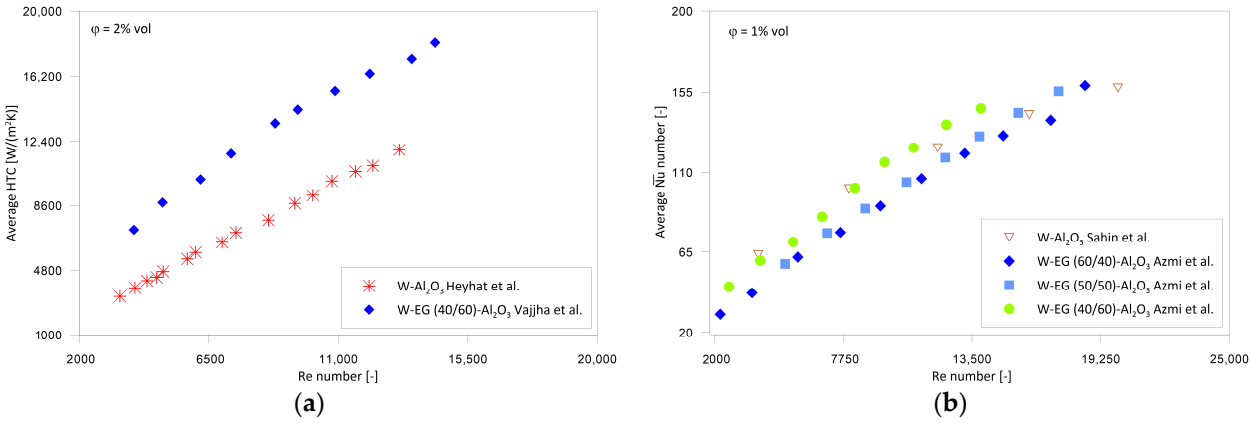

Figure 18. Comparison of different base fluid–Al_2O_3 studies during transition–turbulent flow; (**a**) $\overline{h} = f(Re)$; and (**b**) $\overline{Nu} = f(Re)$ [65,78,93,111].

Figure 18a shows that HTC obtained by Vajjha et al. [65] for water–EG(40/60)–Al_2O_3 nanofluid was distinctly higher than that determined by Heyhat et al. [78] for water–Al_2O_3 nanofluid for the same NPs concentration and the same Re number. Figure 18b displays that for Re < 7800, so for transition flow, regardless of the water–EG ratio, i.e., water content in the water–EG mixture, the average Nu number determined by Azmi et al. [111] for water–EG mixture–Al_2O_3 nanofluid was lower than that determined by Sahin et al. [93] for water–Al_2O_3 nanofluid. However, for Re > 10,000, so for turbulent flow, the average Nu number determined by Azmi et al. [111] for water–EG mixture–Al_2O_3 nanofluid with lower water content was higher than that determined by Sahin et al. [93] for water–Al_2O_3 nanofluid.

Figure 19 compares available experimental data for TiO_2 nanoparticles in transition–turbulent flow in the form of average $\overline{Nu}$ number as a function of Re number.

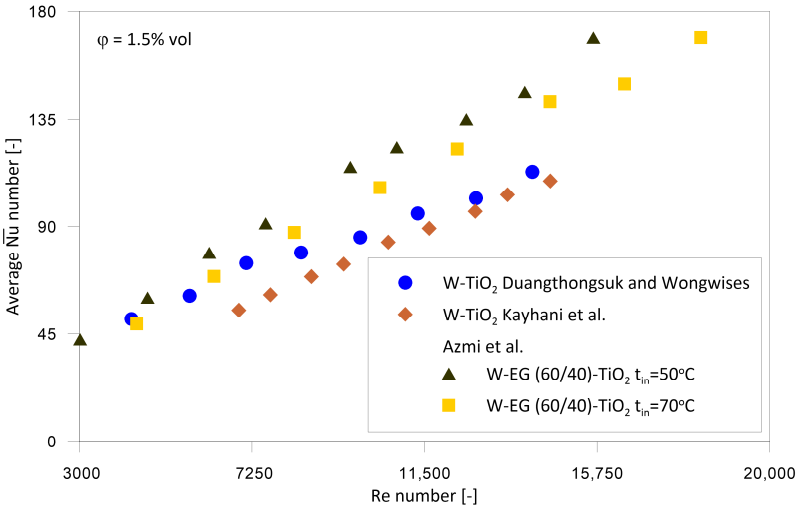

Figure 19. Comparison of $\overline{Nu} = f(Re)$ relationship for different base fluid–TiO_2 studies during transition–turbulent flow [61,79,136].

Figure 19 shows that regardless of the inlet temperature, the average $\overline{Nu}$ number determined by Azmi et al. [136] for water–EG(60/40)–TiO_2 nanofluid was higher than that determined by Duangthongsuk and Wongwises [61] and Kayhani et al. [79] for water–TiO_2 nanofluid.

Figure 20 compares available experimental data for SiO_2 nanoparticles in transition–turbulent flow in the form of average Nu number as a function of Re number.

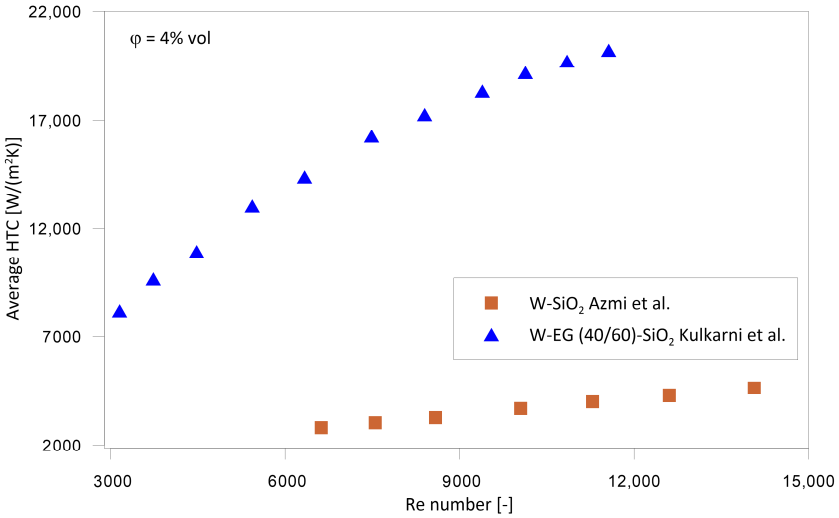

Figure 20. Comparison of $\overline{h} = f(Re)$ relationship for different base fluid–SiO_2 studies during transition–turbulent flow [51,100].

Figure 20 shows that the average HTC determined by Kulkarni et al. [51] for water–EG(40/60)–SiO_2 nanofluid was almost an order of magnitude higher than that determined by Azmi et al. [100] for water–SiO_2 nanofluid for the same NPs concentration and the same Re number.

Figure 21 compares available experimental data for CuO nanoparticles in laminar flow in the form of average HTC as a function of Re number.

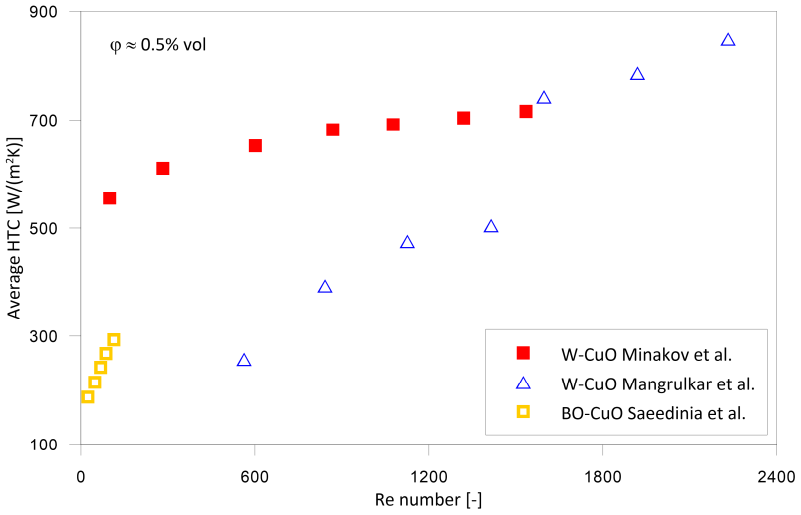

Figure 21. Comparison of $\overline{h} = f(Re)$ relationship for different base fluid–CuO studies during laminar flow [83,118,132].

Figure 21 shows that the average HTC determined by Saeedinia et al. [83] for BO–CuO nanofluid was distinctly lower than that determined by Minakov et al. [118] and Mangrulkar et al. [132] for water–CuO nanofluid. Due to the very high viscosity of the base oil (BO), i.e., almost two orders of magnitude higher than that of water, Saeedinia et al. [83] conducted their research for very small Re numbers.

Figure 22 compares available experimental data for Ag nanoparticles in transition–turbulent regime in the form of average $\overline{Nu}$ number as a function of Re number.

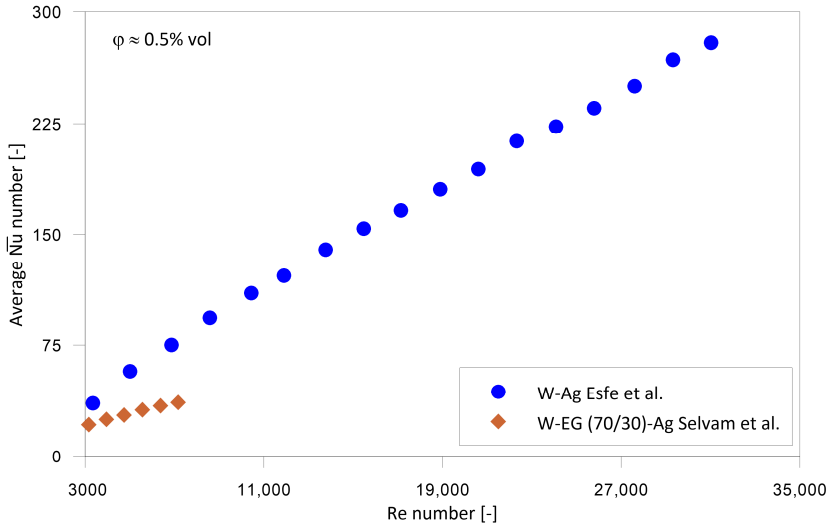

Figure 22. Comparison of $\overline{Nu} = f(Re)$ relationship for different base fluid–Ag studies during transition–turbulent flow [125,129].

Figure 22 shows that the average $\overline{Nu}$ number determined by Selvam et al. [129] for water–EG(70/30)–Ag nanofluid was in good agreement with that determined by Esfe et al. [125] for water–Ag nanofluid and for lower Re number. However, for higher Re number, the average $\overline{Nu}$ number determined by Esfe et al. [125] was higher than that determined by Selvam et al. [129], and the discrepancy increased with Re number increase.

Figure 23 compares available experimental data for MWCNT nanoparticles in laminar–transition flow in the form of average HTC as a function of Re number.

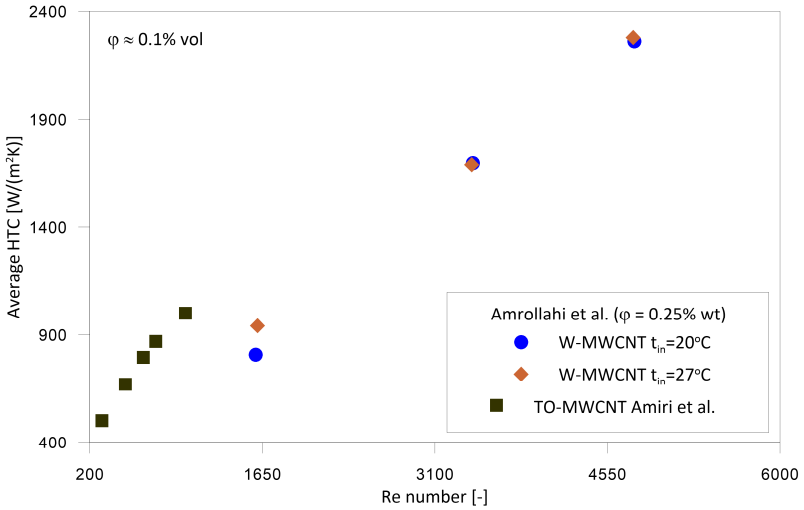

Figure 23. Comparison of $\overline{h} = f(Re)$ relationship for different base fluid–MWCNT studies during laminar–transition flow [66,116].

Figure 23 shows that the average HTC determined by Amrollahi et al. [66] for water–MWCNT nanofluid, regardless of the inlet temperature, displayed the same slope as the results determined by Amiri et al. [116] for very viscous TO–MWCNT nanofluid.

4. Conclusions

As the presented analysis shows, despite research conducted for almost three decades, there is still no consensus as to the effect of NPs on heat transfer under conditions of forced convection.

Most studies indicate an intensification of heat transfer as a result of adding nanoparticles to the base fluid. However, there are studies that indicate a deterioration of heat transfer as a result of adding nanoparticles to the base liquid, particularly during laminar mixed convection [96,117]. There are also studies that show that there is a certain optimum concentration of NPs, above or below which heat transfer deteriorates compared to the base fluid [45,52,61,87,100,101]. Finally, there is a group of researchers who have not observed any effect of nanoparticles on the intensity of heat transfer [50,56,113,122,142].

It should be clearly stated that there are several methods to assess the effect of NPs on the intensification of heat transfer. The ratio of the average Nu number for the nanofluid to the average Nu number for the base liquid for the same Re number is most often compared. The ratio of average HTC for nanofluid to average HTC for base fluid for the same Re number or mean fluid velocity is less frequently compared. However, as demonstrated by the pioneering research of Pak and Cho [40], while the Nu number indicated the intensification of heat transfer with increasing concentration of NPs, the HTC for the highest tested concentration of NPs was lower than for the base fluid for the condition of the same velocity. This relationship was also confirmed by the research results presented in [88]. Therefore, some investigators postulate using average velocity as a benchmark [101,105,110,131]. There is also a group of researchers who believe that the comparison criterion should be the same pumping power in the case of nanofluids and base fluids [91,104,110]. Other researchers suggest using as a comparative criterion the same flow rate [118,124,135] or product of the mass flow rate and specific heat [151] as a parameter in the design of heat exchangers.

There is also disagreement among researchers whether the conventional correlations used for calculations for base liquids can be applied to nanofluids. One group of researchers believes that classical correlation equations can be used in the case of nanofluids, provided that the effective thermophysical properties of nanofluids are correctly determined [50,71,78,79,82,91,110–112,118,122,137,142,156]. The second group of researchers is convinced that classical correlations incorrectly predict the Nu

number of nanofluids, even when effective thermophysical properties for nanofluids are used [42–44,46,55,57,62,95]; therefore, new correlations dedicated to nanofluids have been developed—see Tables 2–4.

An important research problem is also the mutual relationship between the influence of NPs on thermal conductivity and HTC. A large group of researchers found that the increase in HTC is much higher than the increase in thermal conductivity [53,57,80,83,89,90,127]. In turn, in [115] it was found that the increase in thermal conductivity was greater than the increase in HTC. In [122] it was found that there was an increase in thermal conductivity, while HTC remained unchanged. Finally, in [126,142] it was found that the increase in thermal conductivity and HTC is of the same order within the measurement error accuracy.

There is also no consensus among researchers as to the impact of NPs on the intensification of heat transfer for individual flow regimes. For laminar flow, an increase in HTC was most frequently observed, especially in the entrance region [43,44,48,53,57,62,67,76,81,90,92,94,95,107,124,150]. However, if the same pumping power was used as a comparative criterion instead of the same Re number or the same velocity, it turned out that the HTC was lower for the nanofluid than for the base fluid [91,110]. In the case of applying the comparative criterion in the form of product of the mass flow rate and specific heat, the HTC for the nanofluid and the base fluid was the same [151]. For the transition flow regime, both an increase [60,129] and a decrease [94] and no change of HTC were observed. In the case of turbulent flow, the vast majority of studies indicate a significant intensification of heat transfer compared to base fluids [42,55,61,63,68–70,74,77,82,87,88,93,105,121,129,135,140,141,144,149,152–155]. Only a few studies show no HTC change or a slight improvement [50,79,94,125]. However, the use of the product of the mass flow rate and specific heat as a comparative criterion shows a deterioration in heat transfer for nanofluids [151].

From the point of view of the division into laminar, transition, and turbulent flow, the results show that critical Re number corresponding to the onset of turbulence is for nanofluids lower than for base fluids and decreases with NPs concentration increase [88,151,154]. This is very important information due to the more intense heat transfer during turbulent flow.

The available test results achieved in different centers for the same nanoparticles, with the same concentration, and for the same flow conditions, but with different base fluids were compared.

The created database should also allow for the development of reliable correlation equations for calculating the HTC.

5. Future Research Directions

As can be seen from the presented literature review, heat transfer under conditions of forced convection of nanofluids has been studied in many aspects. Unfortunately, only some of the results of these studies were used in the comparative analysis. The main reason for not including others was the insufficient description of the conditions of the experiment. While the description of the test procedure is usually sufficient, the descriptions of the heating section do not always include all information regarding, for example, the length of the tube or wall thickness.

The thermal conditions of the experiment are extremely important. Mandatory information should include the temperature at the inlet to the heating section, as well as the average temperature from the inlet and outlet. In the case of electric heating, information on the difference between the energy balance from the nanofluid side and the supplied electric power should be provided. The basic information that should be provided includes the nanofluid mass flow rate or, directly, the average velocity. It is extremely important to determine the degree of intensification of heat transfer in relation to the condition of not only the same Re number or the same velocity, but also the same pumping power.

The issue of fundamental importance is the development of a universal test for the stability of the produced nanofluids.

Due to the role of thermophoresis as a mechanism of intensification of convective heat transfer, it is important to carry out systematic studies in the case of cooling and heating of the same nanofluid, in the same tube, and under the same hydrodynamic conditions.

Intercomparative tests as presented in [110] should be preferred.

Author Contributions: Conceptualization and methodology, J.T.C.; software, P.K.; validation, J.T.C. and P.K.; formal analysis, J.T.C.; investigation, P.K.; resources, J.T.C.; data curation, P.K.; writing—original draft preparation, J.T.C.; writing—review and editing, J.T.C. and P.K. All authors have read and agreed to the published version of the manuscript.

Funding: This research received no external funding.

Institutional Review Board Statement: Not applicable.

Informed Consent Statement: Not applicable.

Data Availability Statement: Not applicable.

Conflicts of Interest: The authors declare no conflict of interest.

Nomenclature

a	Thermal diffusivity	(m^2/s)
d	Diameter	(m)
D	Inside tube diameter	(m)
h	Local heat transfer coefficient	($W/(m^2K)$)
$\overline{h}$	Average heat transfer coefficient	($W/(m^2K)$)
k	Thermal conductivity	(W/(mK))
l	Length of nanotube	(m)
L	Length of tube	(m)
$Nu = \frac{hD}{k}$	Local Nusselt number	(-)
$\overline{Nu} = \frac{\overline{h}D}{k}$	Average Nusselt number	(-)
P	Electrical heating power	(W)
$Pe = RePr$	Peclet number	(-)
$Pr = \frac{v}{a}$	Prandtl number	(-)
q	Heat flux	(W/m^2)
$Re = \frac{uD}{v}$	Reynolds number	(-)
t	Temperature	(°C)
T	Temperature	(K)
u	Velocity	(m/s)
x	Distance from the tube inlet	(m)
Greek symbols		
δ	Thickness	(m)
ν	Kinematic viscosity	(m^2/s)
φ	Nanoparticle concentration	(-)
Subscripts		
av	Average	
B	Blasius	
DB	Dittus–Boelter	
in	Inlet; inside	
nf	Nanofluid	
out	Outside	
p	Particle	
r	Reduced	
ref	Reference	
w	Wall	
Abbreviations		
AA	Acetic acid	
AC	Alternating current	
AG	Arabic gum	

AOM	Alkaline oxidation media
ApH	Adjusted pH
ATF	Automatic transmission fluid
BO	Base oil
BR	Based ratio of water to EG
CNT	Carbon nanotubes
CS	Continuous sonication
CTAB	Cetyl trimethyl ammonium bromide
DC	Direct current
EG	Ethylene glycol
EO	Engine oil
FAS	Fatty acid salt
FGNP	Functionalized GNP
FGO	Functionalized GO
FNPs	Functionalized nanoparticles
GNP	Graphene nanoplatelet
GO	Graphite oxide
GNS	Graphene nanosheets
HA	Hexylamine
hBN	Hexagonal boron nitride
HTO	Heat transfer oil
IP	Isopropanol
KPS	Potassium persulfate
MWCNT	Multi-walled carbon nanotubes
ND	Nanodiamond
NPs	Nanoparticles
NPC	Nanoparticle concentration
ns	Not specified
OHTC	Overall heat transfer coefficient
P	Proprietary
PAAS	Polyacrylic acid ammonium salt
PACSS	Polyacrylic acid copolymer sodium salt
PG	Propylene glycol
PVA	Poly vinyl alcohol
PVP	Poly vinyl pyrrolidone
SD	Sodium deoxycholate
SDBS	Sodium dodecylbenzene sulfonate
SDS	Sodium dodecyl sulfate
SL	Sodium laurate
SO	Synthetic oil
SP	Sodium polycarboxylate
SS	Stainless steel
TO	Turbine oil
vol.	Volume
wt	Mass
W	Water
WS	Without sonication
XGP	Xanthane gum biopolymer

References

1. Choi, S. Enhancing thermal conductivity of fluids with nanoparticles. In *Developments and Applications of Non-Newtonian Flows*; ASME: New York, NY, USA, 1995; Volume 231, pp. 99–105.
2. Sharma, P.; Sharma, S.; Gangacharyulu, D. Review on thermal properties of nanofluids and factors affecting the same. *Int. J. Eng. Sci. Technol.* **2014**, *6*, 502–519.

3. Angayarkanni, S.A.; John Philip, J. Review on thermal properties of nanofluids: Recent developments. *Adv. Colloid Interface Sci.* **2015**, *225*, 146–176. [CrossRef] [PubMed]
4. Kleinstreuer, C.; Feng, Y. Experimental and theoretical studies of nanofluid thermal conductivity enhancement: A review. *Nanoscale Res. Lett.* **2011**, *6*, 229. [CrossRef] [PubMed]
5. Aybar, H.Ş.; Sharifpur, M.; Azizian, M.R.; Mehrabi, M.; Meyer, J.P. A Review of Thermal Conductivity Models for Nanofluids. *Heat Transf. Eng.* **2015**, *36*, 1085–1110. [CrossRef]
6. Das, P.K. A review based on the effect and mechanism of thermal conductivity of normal nanofluids and hybrid nanofluids. *J. Mol. Liq.* **2017**, *240*, 420–446. [CrossRef]
7. Buongiorno, J.; Hu, L.H.; Kim, S.J.; Hannink, R.; Truong, B.; Forrest, E. Nanofluids for Enhanced Economics and Safety of Nuclear Reactors: An Evaluation of the Potential Features, Issues, and Research Gaps. *Nucl. Technol.* **2008**, *162*, 80–91. [CrossRef]
8. Mukherjee, S.; Ebrahim, S.; Mishra, P.C.; Ali, N.; Chaudhuri, P. A Review on Pool and Flow Boiling Enhancement Using Nanofluids: Nuclear Reactor Application. *Processes* **2022**, *10*, 177. [CrossRef]
9. Colangelo, G.; Favale, E.; Milanese, M.; de Risi, A.; Laforgia, D. Cooling of electronic devices: Nanofluids contribution. *Appl. Therm. Eng.* **2017**, *127*, 421–435. [CrossRef]
10. Bahiraei, M.; Heshmatian, S. Electronics cooling with nanofluids: A critical review. *Energy Conv. Manag.* **2018**, *172*, 438–456. [CrossRef]
11. Almertejy, A.; Rashid, M.M.; Ali, N.; Almurtaji, S. Application of Nanofluids in Gas Turbine and Intercoolers—A Comprehensive Review. *Nanomaterials* **2022**, *12*, 338. [CrossRef]
12. Jinsiwale, N.; Achwal, V. Heat Transfer Enhancement in Automobile Radiator Using Nanofluids: A Review. *Int. J. Eng. Trends Technol.* **2018**, *55*, 68–74. [CrossRef]
13. Abbas, F.; Ali, H.M.; Shah, T.R.; Babar, H.; Janjua, M.M.; Sajjad, U.; Amer, M. Nanofluid: Potential evaluation in automotive radiator. *J. Mol. Liq.* **2020**, *297*, 112014. [CrossRef]
14. Nemova, G.; Filho, E.S.L.; Loranger, S.; Kashyap, R. Laser cooling with nanoparticles. In *Photonics North*; SPIE: Bellingham, WA, USA, 2012; Volume 8412.
15. Sidik, N.A.C.; Yazid, M.N.A.W.M.; Mamat, R. A review on the application of nanofluids in vehicle engine cooling system. *Int. Commun. Heat Mass Transf.* **2015**, *68*, 85–90. [CrossRef]
16. Islam, M.R.; Shabani, B.; Rosengarten, G.; Andrews, J. The potential of using nanofluids in PEM fuel cell cooling systems: A review. *Renew. Sustain. Energy Rev.* **2015**, *48*, 523–539. [CrossRef]
17. Esfe, M.H.; Afran, M. A review on fuel cell types and the application of nanofluid in their cooling. *J. Therm. Anal. Calorim.* **2020**, *140*, 1633–1654. [CrossRef]
18. Abdelkareem, M.A.; Mahmoud, M.S.; Elsaid, K.; Sayed, E.T.; Wilberforce, T.; Al-Murisi, M.; Maghrabie, H.M.; Olabi, A.G. Prospects of Thermoelectric Generators with Nanofluid. *Therm. Sci. Eng Prog.* **2022**, *29*, 101207. [CrossRef]
19. Mohaghegh, M.R. Nanofluids Applications in Solar Energy Systems: A Review. *J. Sol. Energy Res.* **2018**, *3*, 57–65.
20. Khanafer, K.; Vafai, K. A review on the applications of nanofluids in solar energy field. *Renew. Energy* **2018**, *123*, 398–406. [CrossRef]
21. Wahab, A.; Hassan, A.; Qasim, M.A.; Ali, H.M.; Babar, H.; Sajid, M.U. Solar energy systems—Potential of nanofluids. *J. Mol. Liq.* **2019**, *289*, 111049. [CrossRef]
22. Huminic, G.; Huminic, A. Application of nanofluids in heat exchangers: A review. *Renew. Sustain. Energy Rev.* **2012**, *16*, 5625–5638. [CrossRef]
23. Kamthe, S.S.; Barve, S.B. Effect of different nanofluids on performance of shell and tube heat exchanger: A review. *Int. J. Res. Eng. Technol.* **2017**, *6*, 38–41.
24. Menni, Y.; Chamkha, A.J.; Ameur, H. Advances of nanofluids in heat exchangers—A review. *Heat Transf.* **2020**, *49*, 4321–4349. [CrossRef]
25. Pandya, N.S.; Shah, H.; Molana, M.; Tiwari, A.K. Heat transfer enhancement with nanofluids in plate heat exchangers: A comprehensive review. *Eur. J. Mech. B/Fluids* **2020**, *81*, 173–190. [CrossRef]
26. Taylor, R.; Coulombe, S.; Otanicar, T.; Phelan, P.; Gunawan, A.; Lv, W.; Rosengarten, G.; Prasher, R.; Tyagi, H. Small particles, big impacts. A review of the diverse applications of nanofluids. *J. Appl. Phys.* **2013**, *113*, 011301. [CrossRef]
27. Sajid, M.U.; Ali, H.M. Recent advances in application of nanofluids in heat transfer devices: A critical review. *Renew. Sustain. Energy Rev.* **2019**, *103*, 556–592. [CrossRef]
28. Okonkwo, E.C.; Wole-Osho, I.; Almanassra, I.W.; Abdullatif, Y.M.; Al-Ansari, T. An updated review of nanofluids in various heat transfer devices. *J. Therm. Anal. Calorim.* **2021**, *145*, 2817–2872. [CrossRef]
29. Gupta, M.; Arora, N.; Kumar, R.; Kumar, S.; Dilbaghi, N. A comprehensive review of experimental investigations of forced convective heat transfer characteristics for various nanofluids. *Int. J. Mech. Mater. Eng.* **2014**, *9*, 11. [CrossRef]
30. Sidik, N.A.C.; Samion, S.; Musa, M.N.; Muhammad, M.J.; Muhammad, A.I.; Yazid, M.N.A.W.M.; Mamat, R. The significant effect of turbulence characteristics on heat transfer enhancement using nanofluids: A comprehensive review. *Int. Commun. Heat Mass Transf.* **2016**, *72*, 39–47. [CrossRef]
31. Kakaç, S.; Pramuanjaroenkij, A. Single-phase and two-phase treatments of convective heat transfer enhancement with nanofluids—A state-of-the-art review. *Int. J. Therm. Sci.* **2016**, *100*, 75–97. [CrossRef]

32. Liang, G.; Mudawar, I. Review of single-phase and two-phase nanofluid heat transfer in macro-channels and micro-channels. *Int. J. Heat Mass Transf.* **2019**, *136*, 324–354. [CrossRef]
33. Bakthavatchalam, B.; Habib, K.; Saidur, R.; Saha, B.B.; Irshad, K. Comprehensive study on nanofluid and ionanofluid for heat transfer enhancement: A review on current and future perspective. *J. Mol. Liq.* **2020**, *305*, 112787. [CrossRef]
34. Narankhishig, Z.; Ham, J.; Lee, H.; Cho, H. Convective heat transfer characteristics of nanofluids including the magnetic effect on heat transfer enhancement—A review. *Appl. Therm. Eng.* **2021**, *193*, 116987. [CrossRef]
35. Colangelo, G.; Diamante, N.F.; Milanese, M.; Starace, G.; de Risi, A. A Critical Review of Experimental Investigations about Convective Heat Transfer Characteristics of Nanofluids under Turbulent and Laminar Regimes with a Focus on the Experimental Setup. *Energies* **2021**, *14*, 6004. [CrossRef]
36. Awais, M.; Ullah, N.; Ahmad, J.; Sikandar, F.; Ehsan, M.M.; Salehin, S.; Bhuiyan, A.A. Heat transfer and pressure drop performance of nanofluid: A state-of- the-art review. *Int. J. Thermofluids* **2021**, *9*, 100065. [CrossRef]
37. Dittus, F.W.; Boelter, L.M.K. Heat transfer in automobile radiators of the tubular type. *Univ. Calif. Publ. Eng.* **1930**, *2*, 443–461. [CrossRef]
38. Kraußold, H. Die Wärmeübertragung an Flüssigkeiten in Rohren bei turbulenter Strömung. *Forsch. Geb. Ing.* **1933**, *4*, 39–44. [CrossRef]
39. Sieder, E.N.; Tate, G.E. Heat transfer and pressure drop of liquids in tubes. *Ind. Eng. Chem.* **1936**, *28*, 1429–1435. [CrossRef]
40. Pak, B.C.; Cho, Y.I. Hydrodynamic and heat transfer study of dispersed fluids with submicron metallic oxide particles. *Exp. Heat Transf.* **1998**, *11*, 151–170. [CrossRef]
41. Li, Q.; Xuan, Y. Convective heat transfer and flow characteristics of Cu-water nanofluid. *Sci. China Ser. E-Technol. Sci.* **2002**, *45*, 408–416.
42. Xuan, Y.; Li, Q. Investigation on Convective Heat Transfer and Flow Features of Nanofluids. *J. Heat Transf.* **2003**, *125*, 151–155. [CrossRef]
43. Wen, D.; Ding, Y. Experimental investigation into convective heat transfer of nanofluids at the entrance region under laminar flow conditions. *Int. J. Heat Mass Transf.* **2004**, *47*, 5181–5188. [CrossRef]
44. Yang, Y.; Zhang, Z.G.; Grulke, E.A.; Anderson, W.B.; Wu, G. Heat transfer properties of nanoparticle-in-fluid dispersions (nanofluids) in laminar flow. *Int. J. Heat Mass Transf.* **2005**, *48*, 1107–1116. [CrossRef]
45. Kabelac, S.; Kuhnke, J.F. Heat transfer mechanisms in nanofluids—Experiments and theory. In Proceedings of the International Heat Transfer Conference, Sydney, Australia, 13–18 August 2016; Begel House Inc.: Sydney, Australia, 2006.
46. Heris, S.Z.; Etemad, S.G.; Esfahany, M.N. Experimental investigation of oxide nanofluids laminar flow convective heat transfer. *Int. Commun. Heat Mass Transf.* **2006**, *33*, 529–535. [CrossRef]
47. Heris, S.Z.; Esfahany, M.N.; Etemad, S.G. Investigation of CuO/water nanofluid laminar convective heat transfer through a circular tube. *J. Enhanc. Heat Transf.* **2006**, *13*, 279–289. [CrossRef]
48. Ding, Y.; Alias, H.; Wen, D.; Williams, R.A. Heat transfer of aqueous suspensions of carbon nanotubes (CNT nanofluids). *Int. J. Heat Mass Transf.* **2006**, *49*, 240–250. [CrossRef]
49. Heris, S.Z.; Esfahany, M.N.; Etemad, S.G. Experimental investigation of convective heat transfer of Al_2O_3/water nanofluid in circular tube. *Int. J. Heat Fluid Flow* **2007**, *28*, 203–210. [CrossRef]
50. Williams, W.; Buongiorno, J.; Hu, L.W. Experimental investigation of turbulent convective heat transfer and pressure loss of alumina/water and zirconia/water nanoparticle colloids (nanofluids) in horizontal tubes. *J. Heat Transf.* **2008**, *130*, 042412. [CrossRef]
51. Kulkarni, D.P.; Namburu, P.K.; Bargar, H.E.; Das, D.K. Convective Heat Transfer and Fluid Dynamic Characteristics of SiO_2—Ethylene Glycol/Water Nanofluids. *Heat Transf. Eng.* **2008**, *29*, 1027–1035. [CrossRef]
52. Sommers, A.D.; Yerkes, K.L. Experimental investigation into the convective heat transfer and system-level effects of Al_2O_3-propanol nanofluid. *J. Nanoparticle Res.* **2009**, *12*, 1003–1014. [CrossRef]
53. Kim, D.; Kwon, Y.; Cho, Y.; Li, C.; Cheong, S.; Hwang, Y.; Lee, J.; Hong, D.; Moon, S. Convective heat transfer characteristics of nanofluids under laminar and turbulent flow conditions. *Curr. Appl. Phys.* **2009**, *9*, 119–123. [CrossRef]
54. Anoop, K.B.; Sundararajan, T.; Das, S.K. Effect of particle size on the convective heat transfer in nanofluid in the developing region. *Int. J. Heat Mass Transf.* **2009**, *52*, 2189–2195. [CrossRef]
55. Yu, W.; France, D.M.; Smith, S.; Singh, D.; Timofeeva, E.V.; Routbort, J.L. Heat transfer to a silicon carbide/water nanofluid. *Int. J. Heat Mass Transf.* **2009**, *52*, 3606–3612. [CrossRef]
56. Liao, L.; Liu, Z.H. Forced convective flow drag and heat transfer characteristics of carbon nanotube suspensions in a horizontal small tube. *Heat Mass Transf.* **2009**, *45*, 1129–1136. [CrossRef]
57. Hwang, K.S.; Jang, S.P.; Choi, S.U.S. Flow and convective heat transfer characteristics of water-based Al_2O_3 nanofluids in fully developed laminar flow regime. *Int. J. Heat Mass Transf.* **2009**, *52*, 193–199. [CrossRef]
58. Asirvatham, L.G.; Vishal, N.; Gangatharan, S.K.; Lal, D.M. Experimental study on forced convective heat transfer with low volume fraction of CuO/Water nanofluid. *Energies* **2009**, *2*, 97–119. [CrossRef]
59. Torii, S.; Yang, W. Heat Transfer Augmentation of Aqueous Suspensions of Nanodiamonds in Turbulent Pipe Flow. *ASME J. Heat Transf.* **2009**, *131*, 043203. [CrossRef]

60. Sharma, K.V.; Sundar, L.S.; Sarma, P.K. Estimation of heat transfer coefficient and friction factor in the transition flow with low volume concentration of Al_2O_3 nanofluid flowing in a circular tube and with twisted tape insert. *Int. Commun. Heat Mass Transf.* **2009**, *36*, 503–507. [CrossRef]
61. Duangthongsuk, W.; Wongwises, S. An experimental study on the heat transfer performance and pressure drop of TiO_2-water nanofluids flowing under a turbulent flow regime. *Int. J. Heat Mass Transf.* **2010**, *53*, 334–344. [CrossRef]
62. Mosavian, M.T.H.; Heris, S.Z.; Etemad, S.G.; Esfahany, M.N. Heat transfer enhancement by application of nano-powder. *J. Nanoparticle Res.* **2010**, *12*, 2611–2619. [CrossRef]
63. Fotukian, S.M.; Esfahany, M. Experimental investigation of turbulent convective heat transfer of dilute γ-Al_2O_3/water nanofluid inside a circular tube. *Int. J. Heat Fluid Flow* **2010**, *31*, 606–612. [CrossRef]
64. Fotukian, S.M.; Esfahany, M. Experimental study of turbulent convective heat transfer and pressure drop of dilute CuO/water nanofluid inside a circular tube. *Int. Commun. Heat Mass Transf.* **2010**, *37*, 214–219. [CrossRef]
65. Vajjha, R.S.; Das, D.K.; Kulkarni, D.P. Development of new correlations for convective heat transfer and friction factor in turbulent regime for nanofluids. *Int. J. Heat Mass Transf.* **2010**, *53*, 4607–4618. [CrossRef]
66. Amrollahi, A.; Rashidi, A.M.; Lotfi, R.; Meibodi, M.E.; Kashefi, K. Convection heat transfer of functionalized MWNT in aqueous fluids in laminar and turbulent flow at entrance region. *Int. Commun. Heat Mass Transf.* **2010**, *37*, 717–723. [CrossRef]
67. Xie, H.; Li, Y.; Yu, W. Intriguingly high convective heat transfer enhancement of nanofluid coolants in laminar flows. *Phys. Lett A* **2010**, *374*, 2566–2568. [CrossRef]
68. Baby, T.T.; Ramaprabhu, S. Enhanced convective heat transfer using graphene dispersed nanofluids. *Nanoscale Res. Lett.* **2011**, *6*, 289. [CrossRef] [PubMed]
69. Asirvatham, L.G.; Rajab, B.; Lal, D.M.; Wongwises, S. Convective heat transfer of nanofluids with correlations. *Particuology* **2011**, *9*, 626–631. [CrossRef]
70. Sajadi, A.R.; Kazemi, M.H. Investigation of turbulent convective heat transfer and pressure drop of TiO_2/water nanofluid in circular tube. *Int. Commun. Heat Mass Transf.* **2011**, *38*, 474–1478. [CrossRef]
71. Ferrouillat, S.; Bontemps, A.; Ribeiro, J.P.; Gruss, J.A.; Soriano, O. Hydraulic and heat transfer study of SiO_2/water nanofluids in horizontal tubes with imposed wall temperature boundary conditions. *Int. J. Heat Fluid Flow* **2011**, *32*, 424–439. [CrossRef]
72. Ho, C.J.; Huang, J.B.; Tsai, P.S.; Yang, Y.M. Water-Based Suspensions of Al_2O_3 Nanoparticles and MEPCM Particles on Convection Effectiveness in a Circular Tube. *Int. J. Therm. Sci.* **2011**, *50*, 736–748. [CrossRef]
73. Timofeeva, E.V.; Yu, W.; France, D.M.; Singh, D.; Routbort, J.L. Base fluid and temperature effects on the heat transfer characteristics of SiC in ethylene glycol/H_2O and H_2O nanofluids. *J. Appl. Phys.* **2011**, *109*, 014914. [CrossRef]
74. Chandrasekar, M.; Suresh, S. Experiments to Explore the Mechanisms of Heat Transfer in Nanocrystalline Alumina/Water Nanofluid Under Laminar and Turbulent Flow Conditions. *Exp. Heat Transf.* **2011**, *24*, 234–256. [CrossRef]
75. Abdulhassan, A.K.; Al-Jabair, S.; Sultan, K. Experimental Investigation of Heat Transfer and Flow of Nano Fluids in Horizontal Circular. *Int. J. Mech. Mechatron. Eng.* **2012**, *61*, 484–491.
76. Shokouhi, A.; Keshazarz, A.; Ziabasharhagh, M.; Mojarrad, M.S.; Raveshi, M.R. Experimental investigation of nanofluid convective heat transfer in the entrance region of a circular tube. In Proceedings of the ASME 2012 3rd Micro/Nanoscale Heat & Mass Transfer International Conference MNHMT2012, Atlanta, GA, USA, 3–6 March 2012.
77. Vishwanadula, H.; Nsofor, E.C. Studies on forced convection nanofluid flow in circular conduits. *ARPN J. Eng. Appl. Sci.* **2012**, *7*, 371–376.
78. Heyhat, M.M.; Kowsary, F.; Rashidi, A.M.; Esfehani, S.A.V.; Amrollahi, A. Experimental investigation of turbulent flow and convective heat transfer characteristics of alumina water nanofluids in fully developed flow regime. *Int. Commun. Heat Mass Transf.* **2012**, *39*, 1272–1278. [CrossRef]
79. Kayhani, M.H.; Soltanzadeh, H.; Heyhat, M.M.; Nazari, M.; Kowsary, F. Experimental study of convective heat transfer and pressure drop of TiO_2/water nanofluid. *Int. Commun. Heat Mass Transf.* **2012**, *39*, 456–462. [CrossRef]
80. Nine, M.J.; Rehman, H.; Chung, H.S.; Bae, K.; Jeong, H.M. Effect of Ultrasonic Action on Al_2O_3/Water Dispersion and Thermal Characterization with Convective Heat Transfer. *Nanosci. Nanotechnol. Lett.* **2012**, *4*, 827–834. [CrossRef]
81. Yu, W.; Xie, H.; Li, Y.; Chen, L.; Wang, Q. Experimental investigation on the heat transfer properties of Al_2O_3 nanofluids using the mixture of ethylene glycol and water as base fluid. *Powder Technol.* **2012**, *30*, 14–19. [CrossRef]
82. Julia, J.; Hernández, L.; Martínez-Cuenca, R.; Hibiki, T.; Mondragón, R.; Segarra, C.; Jarque, J. Measurement and modelling of forced convective heat transfer coefficient and pressure drop of Al_2O_3 and SiO_2–water nanofluids. *Proc. J. Phys. Conf. Ser.* **2012**, *395*, 012038. [CrossRef]
83. Saeedinia, M.; Akhavan-Behabadi, M.A.; Razi, P. Thermal and rheological characteristics of CuO-Base oil nanofluid flow inside a circular tube. *Int. Commun. Heat Mass Transf.* **2012**, *39*, 152–159. [CrossRef]
84. Arani, A.A.A.; Amani, J. Experimental study on the effect of TiO_2-water nanofluid on heat transfer and pressure drop. *Exp. Therm. Fluid Sci.* **2012**, *42*, 107–115. [CrossRef]
85. Almohammadi, H.; Vatan, S.N.; Esmaeilzadeh, E.; Motezaker, A.; Nokhosteen, A. Experimental Investigation of Convective Heat Transfer and Pressure Drop of Al_2O_3/Water Nanofluid in Laminar Flow Regime inside a Circular Tube. *World Acad. Sci. Eng. Technol.* **2012**, *68*, 1887–1892.

86. Kumaresan, V.; Khader, S.M.A.; Karthikeyan, S.; Velraj, R. Convective heat transfer characteristics of CNT nanofluids in a tubular heat exchanger of various lengths for energy efficient cooling/heating system. *Int. J. Heat Mass Transf.* **2013**, *60*, 413–421. [CrossRef]
87. Azmi, W.H.; Sharma, K.V.; Sarma, P.K.; Mamat, R.; Anuar, S.; Rao, V.D. Experimental determination of turbulent forced convection heat transfer and friction factor with SiO_2 nanofluid. *Exp. Therm. Fluid Sci.* **2013**, *51*, 103–111. [CrossRef]
88. Meyer, J.P.; McKrell, T.J.; Grote, K. The influence of multi-walled carbon nanotubes on single-phase heat transfer and pressure drop characteristics in the transitional flow regime of smooth tubes. *Int. J. Heat Mass Transf.* **2013**, *58*, 597–609. [CrossRef]
89. Ferrouillat, S.; Bontemps, A.; Poncelet, O.; Soriano, O.; Gruss, J.A. Influence of nanoparticle shape factor on convective heat transfer and energetic performance of water-based SiO_2 and ZnO nanofluids. *Appl. Therm. Eng.* **2013**, *51*, 839–851. [CrossRef]
90. Abreu, B.; Lamas, B.; Fonseca, A.; Martins, N.; Oliveira, M.S.A. Experimental characterization of convective heat transfer with MWCNT based nanofluids under laminar flow conditions. *Heat Mass Transf.* **2013**, *50*, 65–74. [CrossRef]
91. Haghighi, E.B.; Saleemi, M.; Nikkam, N.; Anwar, Z.; Lumbreras, I.; Behi, M.; Mirmohammadi, S.A.; Poth, H.; Khodabandeh, R.; Toprak, M.S.; et al. Cooling performance of nanofluids in a small diameter tube. *Exp. Therm. Fluid Sci.* **2013**, *49*, 114–122. [CrossRef]
92. Paul, T.C.; Visser, A.E.; Morshed, A.K.M.M.; Bridges, N.J.; Fox, E.B.; Khan, J.A. Enhanced Thermal Performance of Ionic Liquid-Al_2O_3 Nanofluid as Heat Transfer Fluid for Solar Collector. In Proceedings of the ASME 7th International Conference on Energy Sustainability ES-Fuel Cell 2013, Minneapolis, MN, USA, 14–19 July 2013.
93. Sahin, B.; Gültekin, G.G.; Manay, E.; Karagoz, S. Experimental investigation of heat transfer and pressure drop characteristics of Al_2O_3-water nanofluid. *Exp. Therm. Fluid Sci.* **2013**, *50*, 21–28. [CrossRef]
94. Wusiman, K.E.B.J.; Chung, H.S.; Md, J.N.; Handry, A.; Eom, Y.S.; Kim, J.H.; Jeong, H.M. Heat transfer characteristics of nanofluid through circular tube. *J. Cent. South Univ.* **2013**, *20*, 142–148. [CrossRef]
95. Heyhat, M.M.; Kowsary, F.; Rashidi, A.M.; Momenpour, M.H.; Amrollahi, A. Experimental investigation of laminar convective heat transfer and pressure drop of water-based Al_2O_3 nanofluids in fully developed flow regime. *Exp. Therm. Fluid Sci.* **2013**, *44*, 483–489. [CrossRef]
96. Feng, Z.Z.; Li, W. Laminar mixed convection of large-Prandtl-number in-tube nanofluid flow, Part I: Experimental study. *Int. J. Heat Mass Transf.* **2013**, *65*, 919–927. [CrossRef]
97. Rayatzadeh, H.R.; Saffar-Avval, M.; Mansourkiaei, M.; Abbassi, A. Effects of continuous sonication on laminar convective heat transfer inside a tube using water–TiO_2 nanofluid. *Exp. Therm. Fluid Sci.* **2013**, *48*, 8–14. [CrossRef]
98. Esmaeilzadeh, E.; Almohammadi, H.; Vatan, S.N.; Omrani, A.N. Experimental investigation of hydrodynamics and heat transfer characteristics of γ-Al_2O_3/water under laminar flow inside a horizontal tube. *Int. J. Therm. Sci.* **2013**, *63*, 31–37. [CrossRef]
99. Meriläinen, A.; Seppala, A.; Saari, K.; Seitsonen, J.; Roukolainen, J.; Puisto, S.; Rostedt, N.; Ala-Nissila, T. Influence of particle size and shape on turbulent heat transfer characteristics and pressure losses in water-based nanofluids. *Int. J. Heat Mass Transf.* **2013**, *61*, 439–448. [CrossRef]
100. Azmi, W.H.; Sharma, K.V.; Sarma, P.K.; Mamat, R.; Najafi, G. Heat transfer and friction factor of water based TiO_2 and SiO_2 nanofluids under turbulent flow in a tube. *Int. Commun. Heat Mass Transf.* **2014**, *59*, 30–38. [CrossRef]
101. Gupta, M.; Kumar, R.; Arora, N.; Kumar, S.; Dilbagi, N. Experimental investigation of the convective heat transfer characteristics of TiO_2/distilled water nanofluids under constant heat flux boundary condition. *J. Braz. Soc. Mech. Sci. Eng.* **2014**, *37*, 1347–1356. [CrossRef]
102. Mojarrad, M.S.; Keshavarz, A.; Ziabasharhagh, M.; Raznahan, M.M. Experimental investigation on heat transfer enhancement of alumina/water and alumina/water–ethylene glycol nanofluids in thermally developing laminar flow. *Exp. Therm. Fluid Sci.* **2014**, *53*, 111–118. [CrossRef]
103. Chiney, A.; Ganvir, V.; Rai, B.; Pradip. Stable nanofluids for convective heat transfer applications. *J. Heat Transf.* **2014**, *136*, 021704. [CrossRef]
104. Haghighi, E.B.; Saleemi, M.; Nikkam, N.; Khodabandeh, R.; Toprak, M.S.; Muhammed, M.; Palm, B. Accurate basis of comparison for convective heat transfer in nanofluids. *Int. Commun. Heat Mass Transf.* **2014**, *52*, 1–7. [CrossRef]
105. Sadeghinezhad, E.; Mehrali, M.; Latibari, S.T.; Mehrali, M.; Kazi, S.N.; Oon, C.S.; Metselaar, H.S.C. Experimental investigation of convective heat transfer using graphene nanoplatelet based nanofluids under turbulent flow conditions. *Ind. Eng. Chem.* **2014**, *53*, 12455–12465. [CrossRef]
106. Ghozatloo, A.; Rashidi, A.; Shariaty-Niassar, M. Convective heat transfer enhancement of graphene nanofluids in shell and tube heat exchanger. *Exp. Therm. Fluid Sci.* **2014**, *53*, 136–141. [CrossRef]
107. Halelfadl, S.; Estellé, P.; Maré, T. Heat transfer properties of aqueous carbon nanotubes nanofluids in coaxial heat exchanger under laminar regime. *Exp. Therm. Fluid Sci* **2014**, *55*, 174–180. [CrossRef]
108. Reddy, M.C.S.; Rao, V.V. Experimental investigation of heat transfer coefficient and friction factor of ethylene glycol water based TiO_2 nanofluid in double pipe heat exchanger with and without helical coil inserts. *Int. Commun. Heat Mass Transf.* **2014**, *50*, 68–76. [CrossRef]
109. Ho, C.J.; Lin, Y.J. Turbulent Forced Convection Effectiveness of Alumina–Water Nanofluid in a Circular Tube With Elevated Inlet Fluid Temperatures: An Experimental Study. *Int. Commun. Heat Mass Transf.* **2014**, *57*, 247–253. [CrossRef]
110. Utomo, A.T.; Haghighi, E.B.; Zavareh, A.I.T.; Ghanbarpourgeravi, M.; Poth, H.; Khodabandeh, R.; Palm, B.; Pacek, A.W. The effect of nanoparticles on laminar heat transfer in a horizontal tube. *Int. J. Heat Mass Transf.* **2014**, *69*, 77–91. [CrossRef]

111. Esfe, M.H.; Saedodin, S.; Mahmoodi, M. Experimental studies on the convective heat transfer performance and thermophysical properties of MgO–water nanofluid under turbulent flow. *Exp. Therm. Fluid Sci.* **2014**, *52*, 68–78. [CrossRef]
112. Akhavan-Zanjani, H.; Saffar-Avval, M.; Mansourkiaei, M.; Ahadi, M.; Sharif, F. Turbulent convective heat transfer and pressure drop of graphene–water nanofluid flowing inside a horizontal circular tube. *J. Dispers. Sci. Technol.* **2014**, *35*, 1230–1240. [CrossRef]
113. Sahin, B.; Manay, E.; Akyurek, E.F. An Experimental Study on Heat Transfer and Pressure Drop of CuO-Water Nanofluid. *J. Nanomater.* **2015**, *16*, 790839. [CrossRef]
114. Akhavan-Behabadi, M.A.; Hekmatipour, F.; Mirhabibi, S.M.; Sajadi, B. Experimental investigation of thermal–rheological properties and heat transfer behavior of the heat transfer oil–copper oxide (HTO–CuO) nanofluid in smooth tubes. *Exp. Therm. Fluid Sci.* **2015**, *68*, 681–688. [CrossRef]
115. Mehrali, M.; Sadeghinezhad, E.; Rosen, M.A.; Akhiani, A.R.; Latibari, S.T.; Mehrali, M.; Metselaar, H.S.C. Heat transfer and entropy generation for laminar forced convection flow of graphene nanoplatelets nanofluids in a horizontal tube. *Int. Commun. Heat Mass Transf.* **2015**, *66*, 23–31. [CrossRef]
116. Amiri, A.; Shanbedi, M.; Yarmand, H.; Arzani, H.K.; Gharehkhani, S.; Montazer, E.; Sadri, R.; Sarsam, W.; Chew, B.; Kazi, S. Laminar convective heat transfer of hexylamine-treated MWCNTs-based turbine oil nanofluid. *Energy Convers. Manag.* **2015**, *105*, 355–367. [CrossRef]
117. Colla, L.; Fedele, L.; Buschmann, M.H. Laminar mixed convection of TiO_2-water nanofluid in horizontal uniformly heated pipe flow. *Int. J. Therm. Sci.* **2015**, *97*, 26–40. [CrossRef]
118. Minakov, A.V.; Lobasov, A.S.; Guzei, D.V.; Pryazhnikov, M.I.; Rudyak, V.Y. The experimental and theoretical study of laminar forced convection of nanofluids in the round channel. *Appl. Therm. Eng.* **2015**, *88*, 140–148. [CrossRef]
119. Sadeghinezhad, E.; Togun, H.; Mehrali, M.; Nejad, P.S.; Latibari, S.T.; Abdulrazzaq, T.; Kazi, S.N.; Metselaar, H.S.C. An experimental and numerical investigation of heat transfer enhancement for graphene nanoplatelets nanofluids in turbulent flow conditions. *Int. J. Heat Mass Transf.* **2015**, *81*, 41–51. [CrossRef]
120. Chavan, D.; Pise, A.T. Experimental investigation of convective heat transfer agumentation using Al_2O_3/water nanofluid in circular pipe. *Heat Mass Transf.* **2015**, *51*, 1237–1246. [CrossRef]
121. Usri, N.N.; Azmi, W.H.; Mamat, R.; Hamid, K.A.K.; Najafib, G. Heat Transfer Augmentation of Al_2O_3 Nanofluid in 60:40 Water to Ethylene Glycol Mixture. *Energy Procedia* **2015**, *79*, 403–408. [CrossRef]
122. Cabaleiro, D.; Colla, L.; Agresti, F.; Lugo, L.; Fedele, L. Transport properties and heat transfer coefficients of ZnO/(ethylene glycol+water) nanofluids. *Int. J. Heat Mass Transf.* **2015**, *89*, 433–443. [CrossRef]
123. Gómez, A.O.C.; Hoffmann, A.R.K.; Filho, E.P.B. Experimental evaluation of CNT nanofluids in single-phase flow. *Int. J. Heat Mass Transf.* **2015**, *86*, 277–287. [CrossRef]
124. Patel, B.J.; Subhedar, D. Experimental Investigation of Heat Transfer through Circular Tube using Al_2O_3/Water-EG Nanofluid. *Int. J. Innov. Sci. Eng. Technol.* **2016**, *2*, 6–10.
125. Esfe, M.H.; Saedodin, S.; Biglari, M.; Rostamian, H. An experimental study on thermophysical properties and heat transfer characteristics of low volume concentrations of Ag-water nanofluid. *Int. Commun. Heat Mass Transf.* **2016**, *74*, 91–97. [CrossRef]
126. Akhavan-Zanjani, H.; Saffar-Avval, M.; Mansourkiaei, M.; Sharif, F.; Ahadi, M. Experimental investigation of laminar forced convective heat transfer of Graphene-water nanofluid inside a circular tube. *Int. J. Therm. Sci.* **2016**, *100*, 316–323. [CrossRef]
127. Hatwar, A.; Kriplani, V.M. Experimental Study of Convective Heat Transfer in a Horizontal Tube Using Nanofluids. *Int. J. Adv. Eng. Res. Sci.* **2016**, *3*, 39–44. [CrossRef] [PubMed]
128. Hekmatipour, F.; Akhavan-Behabadi, M.A.; Sajadi, B. Combined free and forced convection heat transfer of the copper oxide-heat transfer oil (CuO-HTO) nanofluid inside horizontal tubes under constant wall temperature. *Appl. Therm. Eng.* **2016**, *100*, 621–627. [CrossRef]
129. Selvam, C.; Irshad, E.C.M.; Lal, D.M.; Harish, S. Convective heat transfer characteristics of water–ethylene glycol mixture with silver nanoparticles. *Exp. Therm. Fluid Sci.* **2016**, *77*, 188–196. [CrossRef]
130. Zarringhalam, M.; Karimipour, A.; Toghraie, D. Experimental study of the effect of solid volume fraction and Reynolds number on heat transfer coefficient and pressure drop of CuO–Water nanofluid. *Exp. Therm. Fluid Sci.* **2016**, *76*, 342–351. [CrossRef]
131. Gupta, M.; Kumar, R.; Arora, N.; Kumar, S.; Dilbagi, N. Forced Convective Heat Transfer of MWCNT/Water Nanofluid Under Constant Heat Flux: An Experimental Investigation. *Arab. J. Sci. Eng.* **2016**, *41*, 599–609. [CrossRef]
132. Mangrulkar, C.K.; Kriplani, V.M.; Dhoble, A.S. Experimental investigation of convective heat transfer enhancement using alumina/water and copper oxide/ water nanofluids. *Therm. Sci.* **2016**, *20*, 1681–1692. [CrossRef]
133. Solangi, K.H.; Amiri, A.; Luhur, M.R.; Ghavimi, S.A.A.; Zubir, M.N.M.; Kazi, S.N.; Badarudin, A. Experimental investigation of the propylene glycol-treated graphene nanoplatelets for the enhancement of closed conduit turbulent convective heat transfer. *Int. Commun. Heat Mass Transf.* **2016**, *73*, 43–53. [CrossRef]
134. Noghrehabadi, A.; Pourrajab, R. Experimental investigation of forced convective heat transfer enhancement of γ-Al_2O_3/water nanofluid in a tube. *J. Mech. Sci. Technol.* **2016**, *30*, 943–952. [CrossRef]
135. Saxena, R.; Gangacharyulu, D.; Bulasara, V.K. Heat Transfer and Pressure Drop Characteristics of Dilute Alumina-Water Nanofluids in a Pipe at Different Power Inputs. *Heat Trans. Eng.* **2016**, *37*, 1554–1565. [CrossRef]
136. Azmi, W.H.; Hamid, K.A.; Mamat, R.; Sharma, K.V.; Mohamad, M.S. Effects of working temperature on thermo-physical properties and forced convection heat transfer of TiO_2 nanofluids in water—Ethylene glycol mixture. *Appl. Therm. Eng.* **2016**, *106*, 1190–1199. [CrossRef]

137. Martínez-Cuenca, R.; Mondragón, R.; Hernández, L.; Segarra, C.; Jarque, J.C.; Hibiki, T.; Juliá, J.E. Forced-convective heat-transfer coefficient and pressure drop of water-based nanofluids in a horizontal pipe. *Appl. Therm. Eng.* **2016**, *98*, 841–849. [CrossRef]
138. Singh, P.; Gupta, R.; Wanchoo, R.K. Experimental Investigation of Forced Convection of Glycol-Based CuO Nanofluids Flowing Through Straight Tubes and Helical Coils. *J. Nanofluids* **2016**, *6*, 220–231. [CrossRef]
139. Selvam, C.; Balaji, T.; Lal, D.M.; Harish, S. Convective heat transfer coefficient and pressure drop of water-ethylene glycol mixture with graphene nanoplatelets. *Exp. Therm. Fluid Sci.* **2017**, *80*, 67–76. [CrossRef]
140. Ranjbarzadeh, R.; Karimipour, A.; Afrand, M.; Isfahani, A.H.M.; Shirneshan, A. Empirical analysis of heat transfer and friction factor of water/graphene oxide nanofluid flow in turbulent regime through an isothermal pipe. *Appl. Therm. Eng.* **2017**, *126*, 538–547. [CrossRef]
141. Azmi, W.H.; Usri, N.A.; Mamat, R.; Sharma, K.V.; Noor, M.M. Forced convection heat transfer of Al_2O_3 nanofluids for different based ratio of water: Ethylene glycol mixture. *Appl. Therm. Eng.* **2017**, *112*, 707–719. [CrossRef]
142. İlhan, B.; Ertürk, H. Experimental characterization of laminar forced convection of hBN-water nanofluid in circular pipe. *Int. J. Heat Mass Transf* **2017**, *111*, 500–507. [CrossRef]
143. Jumpholkul, C.; Mahian, O.; Kasaeian, A.; Dalkilic, A.S.; Wongwises, S. An experimental study to determine the maximum efficiency index in turbulent flow of SiO_2/water nanofluids. *Int. J. Heat Mass Transf.* **2017**, *112*, 1113–1121. [CrossRef]
144. Sundararaj, A.J.; Pillai, B.C.; Asirvatham, L.G. Convective heat transfer analysis of refined kerosene with alumina particles for rocketry application. *J. Mech. Sci. Technol.* **2018**, *32*, 1685–1691. [CrossRef]
145. Cieśliński, J.T.; Kozak, P. Experimental investigation of forced convection of water/EG-Al_2O_3 nanofluids inside horizontal tube. *E3S Web Conf.* **2018**, *70*, 02004. [CrossRef]
146. Ho, C.J.; Chang, C.Y.; Yan, W.M.; Amani, P. A combined numerical and experimental study on the forced convection of Al_2O_3-water nanofluid in a circular tube. *Int. J. Heat Mass Transf.* **2018**, *120*, 66–75. [CrossRef]
147. Singh, P.; Sharma, P.; Gupta, R.; Wanchoo, R.K. Heat transfer characteristics of propylene glycol/water based magnesium oxide nanofluid flowing through straight tubes and helical coils. *J. Therm. Eng.* **2018**, *4*, 1737–1755. [CrossRef]
148. Singh, P.; Gupta, R.; Wanchoo, R.K. Forced Convective Heat Transfer Studies on Glycol Based Al_2O_3 Nanofluids Flowing Through Straight Tubes and Helical Coils. *J. Nanofluids* **2018**, *7*, 37–51. [CrossRef]
149. Solangi, K.H.; Sharif, S.; Sadiq, I.O.; Hisam, M.J. Experimental and numerical investigations on heat transfer and friction loss of functionalized GNP nanofluids. *Int. J. Mech. Eng. Technol.* **2019**, *10*, 61–77.
150. Singh, P.; Oberoi, A.S.; Nijhawan, P. Experimental heat transfer analysis of copper oxide nanofluids through a straight tube. *Int. J. Adv. Trends Comput. Sci. Eng.* **2019**, *8*, 495–500. [CrossRef]
151. Nikulin, S.; Moita, A.S.; Moreira, A.L.N.; Murshed, S.M.S.; Huminic, A.; Grosu, Y.; Faik, A.; Nieto-Maestre, J.; Khliyeva, O. Effect of Al_2O_3 nanoparticles on laminar, transient and turbulent flow of isopropyl alcohol. *Int. J. Heat Mass Transf.* **2019**, *130*, 1032–1044. [CrossRef]
152. Karabulut, K.; Buyruk, E.; Kilinc, F. Experimental and numerical investigation of convection heat transfer in a circular copper tube using graphene oxide nanofluid. *J. Braz. Soc. Mech. Sci. Eng.* **2020**, *42*, 230. [CrossRef]
153. Kong, M.; Lee, S. Performance evaluation of Al_2O_3 nanofluid as an enhanced heat transfer fluid. *Adv. Mech. Eng.* **2020**, *12*, 1687814020952277. [CrossRef]
154. Demirkir, C.; Ertürk, H. Convective Heat Transfer and Pressure Drop Characteristics of Graphene-Water Nanofluids in Transitional Flow. *arXiv* **2020**, arXiv:2009.10462v1. [CrossRef]
155. Ebaid, M.S.; Ghrair, A.M.; Al-busoul, M. Investigation of heat transfer enhancement using ferro-nanofluids (Fe_3O_4/water) in a heated pipe under the application of magnetic field. *Adv. Mech. Eng* **2022**, *14*, 16878132221102647. [CrossRef]
156. Siddiqi, H.-U.; Qamar, A.; Shaukat, R.; Anwar, Z.; Amjad, M.; Farooq, M.; Abbas, M.M.; Imran, S.; Ali, H.; Khan, T.; et al. Heat transfer and pressure drop characteristics of ZnO/DIW based nanofluids in small diameter compact channels: An experimental study. *Case Stud. Therm. Eng.* **2022**, *39*, 102441. [CrossRef]
157. Singh, P.; Sharma, P.; Gupta, R.; Wanchoo, R.K. Time Scale Analysis for Prediction of Nusselt Number of Nanofluids Flowing Through Straight Tubes: An Experimental Study. *Iran. J. Chem. Chem. Eng.* **2022**, *41*, 291–303.
158. Ghadimi, A.; Metselaar, I.H. The influence of surfactant and ultrasonic processing on improvement of stability, thermal conductivity and viscosity of titania nanofluid. *Exp. Therm. Fluid Sci.* **2013**, *51*, 1–9. [CrossRef]
159. Mahbubul, I.M.; Elcioglu, E.B.; Saidur, R.; Amalina, M.A. Optimization of ultrasonication period for better dispersion and stability of TiO_2–water nanofluid. *Ultrason. Sonochem.* **2017**, *37*, 360–367. [CrossRef] [PubMed]
160. Shah, J.; Ranjan, M.; Gupta, S.K.; Sonvane, Y. Ultrasonication effect on thermophysical properties of Al_2O_3 nanofluids. *AIP Conf. Proc.* **2018**, *1951*, 020008.
161. Asadi, A.; Alarifi, I.M. Effects of ultrasonication time on stability, dynamic viscosity, and pumping power management of MWCNT-water nanofluid: An experimental study. *Sci. Rep.* **2020**, *10*, 15182. [CrossRef]
162. Jehhef, K.A.; Siba, M.A.A.A. Effect of surfactant addition on the nanofluids properties: A review. *Acta Mech. Malays.* **2019**, *2*, 1–19. [CrossRef]
163. Askar, A.H.; Kadham, S.A.; Mshehid, S.H. The surfactants effect on the heat transfer enhancement and stability of nanofluid at constant wall temperature. *Heliyon* **2020**, *6*, e04419. [CrossRef] [PubMed]
164. Wang, J.; Li, G.; Li, T.; Zeng, M.; Sundén, B. Effect of various surfactants on stability and thermophysical properties of nanofluids. *J. Therm. Anal. Calorim.* **2021**, *143*, 4057–4070. [CrossRef]

165. Tang, W.; Zou, C.; Peng, H.; Wang, Y.; Shi, L. Influence of Nanoparticles and Surfactants on Stability and Rheological Behavior of Polymeric Nanofluids and the Potential Applications in Fracturing Fluids. *Energy Fuels* **2021**, *35*, 8657–8671. [CrossRef]
166. Liu, D.; Zhang, X.; Tian, F.; Liu, X.; Yuan, J.; Huang, B. Review on nanoparticle-surfactant nanofluids: Formula fabrication and applications in enhanced oil recovery. *J. Dispers. Sci. Technol.* **2022**, *43*, 745–759. [CrossRef]
167. Xie, H.; Lee, H.; Youn, W.; Choi, M. Nanofluids containing multiwalled carbon nanotubes and their enhanced thermal conductivities. *J. Appl. Phys.* **2003**, *94*, 4967–4971. [CrossRef]